ORIGINAL ARTICLE

Aberrant adenosine signaling in patients with focal cortical dysplasia

Mengyi Guo[1,2] · Jing Zhang[1,2] · Jing Wang[2] · Xiongfei Wang[1,3] · Qing Gao[1] · Chongyang Tang[1,3] · Jiahui Deng[1] · Zhonghua Xiong[1,2] · Xiangru Kong[1] · Yuguang Guan[1,3] · Jian Zhou[1,3] · Detlev Boison[4] · Guoming Luan[1,3] · Tianfu Li[1,2]

Abstract

Focal cortical dysplasia (FCD), a common malformation of cortical development, is frequently associated with pharmacoresistant epilepsy in both children and adults. Adenosine is an inhibitory modulator of brain activity and a prospective anti-seizure agent with potential for clinical translation. Our previous results demonstrated that the major adenosine-metabolizing enzyme adenosine kinase (ADK) was upregulated in balloon cells (BCs) within FCD type IIB lesions, suggesting that dysfunction of the adenosine system is implicated in the pathophysiology of FCD. In our current study, we therefore performed a comprehensive analysis of adenosine signaling in surgically resected cortical specimens from patients with FCD type I and type II via immunohistochemistry and immunoblot analysis. Adenosine enzyme signaling was assessed by quantifying the levels of the key enzymes of adenosine metabolism, i.e., ADK, adenosine deaminase (ADA), and ecto-5'-nucleotidase (CD73). Adenosine receptor signaling was assessed by quantifying the levels of adenosine A_{2A} receptor ($A_{2A}R$) and putative downstream mediators of adenosine, namely, glutamate transporter-1 (GLT-1) and mammalian target of rapamycin (mTOR). Within lesions in FCD specimens, we found that the adenosine-metabolizing enzymes ADK and ADA, as well as the adenosine-producing enzyme CD73, were upregulated. We also observed an increase in $A_{2A}R$ density, as well as a decrease in GLT-1 levels and an increase in mTOR levels, in FCD specimens compared with control tissue. These results suggest that dysregulation of the adenosine system is a common pathologic feature of both FCD type I and type II. The adenosine system might therefore be a therapeutic target for the treatment of epilepsy associated with FCD.

Keywords Focal cortical dysplasia · Epilepsy · Adenosine kinase · Balloon cell · Adenosine A_{2A} receptor

Mengyi Guo, Jing Zhang, and Jing Wang co-first authors who contributed equally to this work.

✉ Guoming Luan
luangm@ccmu.edu.cn

✉ Tianfu Li
tianfuli@ccmu.edu.cn

1   Department of Brain Institute, Center of Epilepsy, Beijing Institute for Brain Disorders, Beijing Key Laboratory of Epilepsy Research, Sanbo Brain Hospital, Capital Medical University, Beijing 100093, China

2   Department of Neurology, Center of Epilepsy, Beijing Institute for Brain Disorders, Sanbo Brain Hospital, Capital Medical University, Beijing 100093, China

3   Department of Neurosurgery, Center of Epilepsy, Beijing Institute for Brain Disorders, Beijing Key Laboratory of Epilepsy Research, Sanbo Brain Hospital, Capital Medical University, Beijing 100093, China

4   Department of Neurosurgery, Robert Wood Johnson & New Jersey Medical Schools, Rutgers University, Piscataway, NJ 08854, USA

Introduction

Focal cortical dysplasia (FCD) is one of many malformations of cortical development and is the most common etiology of drug-resistant focal epilepsy requiring surgical treatment in children [1]. According to the clinicopathological classification system published by the ILAE in 2011 [2], FCD can be classified into three neuropathological subtypes: FCD type I, which is characterized by abnormal lamination and disruption of tissue architecture; FCD type II, which involves cortical dyslamination with either dysmorphic neurons (type IIA) or balloon cells (BCs; type IIB); and FCD type III, which is characterized by cortical lamination abnormalities associated with other epileptogenic brain lesions. The most frequent clinical presentation of FCD is focal epilepsy with clinical onset in childhood, and patients with FCD type I or type II generally present with high seizure frequency [3-5]. The etiology and underlying mechanisms

of FCD-associated epilepsy remain unclear. Most of the pathogenic gene variants found to be associated with FCD type II are in single genes regulating the mammalian target of rapamycin (mTOR) signaling pathway, which is essential for neuronal growth and migration [6, 7]. Along with genetic mutations, an inflammatory milieu also promotes seizures within the malformed cortex [8-10]. In addition, retention of immature γ-aminobutyric acid (GABA) receptors may contribute to hyperexcitability within FCD lesions [11, 12]. Our previous study suggested a novel role for adenosine dysregulation in the pathophysiology of FCD type IIB [13].

Adenosine is an endogenous anticonvulsant and neuroprotective regulator of the brain. It elevates seizure thresholds and terminates seizures via activation of inhibitory adenosine A_1 receptors (A_1Rs), while stimulatory adenosine A_{2A} receptors (A_{2A}Rs) may promote synaptic transmission within a globally inhibited network [14-17]. Imbalance of adenosine receptor activation (decreased A_1R signaling and/or increased A_{2A}R signaling) can aggravate the development and progression of epilepsy [18-20]. A_{2A}Rs in the brain exert a vital function in synaptic plasticity and counteract the inhibition of synaptic transmission mediated by A_1Rs [21, 22]. They are largely activated by adenosine produced by the degradation of adenosine triphosphate (ATP), which is released into the synapse in a frequency-dependent manner, via ecto-5'-nucleotidase (CD73) [23]. Alterations in crosstalk between A_1R and A_{2A}R signaling are possibly associated with seizure generation: prolonged activation of high-affinity A_1Rs can lead to their internalization and a consequent increase in A_{2A}R density[24]. Prolonged A_{2A}R activation in turn leads to inhibition of glutamate transporter-1 (GLT-1) function, which impairs glutamate uptake by astrocytes and leads to increased extracellular glutamate concentration, thus contributing to the enhancement of neuronal excitability, seizures, and neurotoxicity [25, 26]. Our previous study demonstrated that a reduction in GLT-1 levels concomitant with an increase in A_{2A}R density aggravates excitotoxicity and promotes cell death in Rasmussen's encephalitis (RE) [27]. Astrocytic adenosine kinase (ADK), the major adenosine-metabolizing enzyme, is a marker of epileptogenesis and a target for its prevention [28-32]. Increasing clinical evidence from specimens surgically resected from patients with drug-resistant epilepsy has proved that maladaptive changes in adenosine system contributes to seizure generation in human chronic epilepsy [31, 33-35]. In our previous studies, we found that ADK density was increased in BCs within FCD type IIB lesions, suggesting that upregulation of ADK is a common pathologic component of FCD type IIB [13]. In addition, the nuclear subtype of ADK may participate in the regulation of cell proliferation through a combination of epigenetic mechanisms and adenosine receptor-dependent interactions with the mTOR pathway [36-38].

Given the putative role of adenosine signaling in the pathophysiology of FCD, we performed a comprehensive analysis of adenosine signaling and its downstream pathways in human specimens derived from surgically resected material from patients with FCD type I and type II.

Materials and methods

Patients and diagnosis

The local ethics committee (Beijing Sanbo Hospital, Capital Medical University, Beijing, China) approved all studies, and clinical investigations were conducted according to the Declaration of Helsinki. Informed consent was obtained from the parents or legal guardians of all participants. Twelve FCD type I (six FCD type IA and six FCD type IB) and twelve FCD type II (six FCD type IIA and six FCD type IIB) patients diagnosed according to typical clinical, magnetic resonance imaging, and neuropathologic findings, as proposed by Palmini et al [39], were enrolled in this study. Presurgical evaluation was performed according to previously described procedures, including MRI (spin−echo T1-weighted axial, T2-weighted axial, coronal and fluid-attenuated inversion recovery imaging of 5-mm-thick axial, sagittal, and coronal sections), fluorodeoxyglucose-positron emission tomography (FDG-PET), scalp video-electroencephalography (EEG), intracranial EEG monitoring, seizure semiology analysis, and neuropsychological testing, at Sanbo Brain Hospital [13, 33, 34, 40]. Interictal/ictal scalp EEG was performed for all patients using a video-EEG monitoring system (Nicolet vEEG; Viasys Healthcare, Madison, USA), with electrodes placed according to the international 10–20 system. The main ictal manifestations were diagnosed according to the semiology classification [41, 42].

FCD subtypes were identified according to data in the neuropathology archives of Beijing Sanbo Brain Hospital collected between August 2011 and August 2012. All patients were diagnosed with pharmacoresistant epilepsy and underwent surgical resection (Table 1). Among patients with FCD type IA, type IB, type IIA, type IIB, the mean ages at seizure onset were 15.9±8.4 years, 6.7±6.1 years, 7.0±5.3 years, and 2.8±1.5 years, respectively; the mean ages at surgery were 27.8±6.9 years, 16.2±7.2 years, 18.0±6.7 years, and 12.0±11.0 years, respectively; and the durations from seizure onset to operation were 9.9±8.4 years, 9.5±7.2 years, 11.0±7.3 years, and 9.3±9.6 years, respectively. The seizure types of patients included simple partial seizures, complex partial seizures, and secondary generalized tonic−clonic seizures. The long-term video EEG results were abnormal in all cases. None of the patients had other relevant epilepsy etiologies before the onset of the disease. The clinical details of the patient cohort were

Table 1 Clinical characteristics of FCD and control cohorts.

Patient Group	Gender	Age at First Seizure, Years	Seizure Types	Duration From Seizure Onset to First Operation, Years	Age at Operation, Years	Operation/Lesion Location
FCD IA						
1	F	14	SPS+GTCS	10	24	Left temporal lobe
2	M	27	SPS+CPS	4	31	Left temporal lobe
3	M	4	SPS+GTCS	22	26	Left temporal lobe
4	M	15	SPS+CPS+GTCS	13	38	Left temporal lobe
5	M	19.5	SPS+GTCS	0.5	20	Right temporal lobe
6	M	10	CPS+GTCS	4	14	Right temporal lobe
FCD IB						
1	M	11	SPS+GTCS	1	12	Left temporal lobe
2	M	0.4	SPS	9.6	10	Right parietal and occipital lobes
3	F	15	SPS+CPS+GTCS	8	23	Right temporal lobe
4	F	3	SPS+GTCS	8	11	Right frontal lobe
5	M	4	SPS+GTCS	21	25	Right temporal lobe
6	F	21	CPS+GTCS	9	30	Right temporal lobe
FCD IIA						
1	M	12	SPS+CPS+GTCS	10	22	Left parietal and occipital lobes
2	M	0	SPS+CPS+GTCS	19	19	Left parietal and occipital lobes
3	M	12	SPS+GTCS	1	13	Right frontal lobe
4	M	1	SPS	8	9	Left parietal and occipital lobes
5	F	9	SPS+GTCS	8	17	Left temporal lobe
6	M	8	SPS+CPS+GTCS	20	28	Right parietal lobe
FCD IIB						
1	M	2	CPS	2	4	Right frontal lobe
2	M	1.5	CPS+GTCS	0.5	2	Right frontal lobe
3	F	3	SPS+GTCS	9	12	Right parietal and occipital lobes
4	M	5	CPS	20	25	Right frontal lobe
5	M	4	SPS+CPS+GTCS	22	26	Right frontal lobe
6	M	1	SPS+GTCS	2	3	Right frontal lobe

SPS, simple partial seizure; CPS, complex partial seizure; GTCS, generalized tonic-clonic seizure; F, female; M, male.

summarized in Table 1. The representative EEG and MRI results of FCD patients were shown in Fig. 1. All resected tissues were paraffin embedded. In addition, portions of the tissues from four patients with each FCD subtype were cryoprotected for Western blot analysis.

For comparison, six neocortical specimens were obtained from well outside the epileptogenic lesion (normal appearing cortex/white matter adjacent to the lesion) from patients with FCD type IIB undergoing resection for pharmacoresistant epilepsy. Of note, microscopic evaluation of those areas was performed to confirm that there were no microscopic changes related to dysplasia to avoid the use of perilesion tissue within the border zone between the lesion and normal-appearing cortex, as the extent of neuropathological abnormalities in this area may vary among subjects [34].

Tissue preparation

Formalin-fixed, paraffin-embedded tissue samples (one representative paraffin block per patient containing the complete lesion or the largest part of the lesion resected at surgery) were sectioned at a thickness of 4 μm and mounted on precoated glass slides (Star Frost, WaldemarKnittel GmbH, Braunschweig, Germany). Sections of all specimens selected in the regions from the most severe lesions were processed
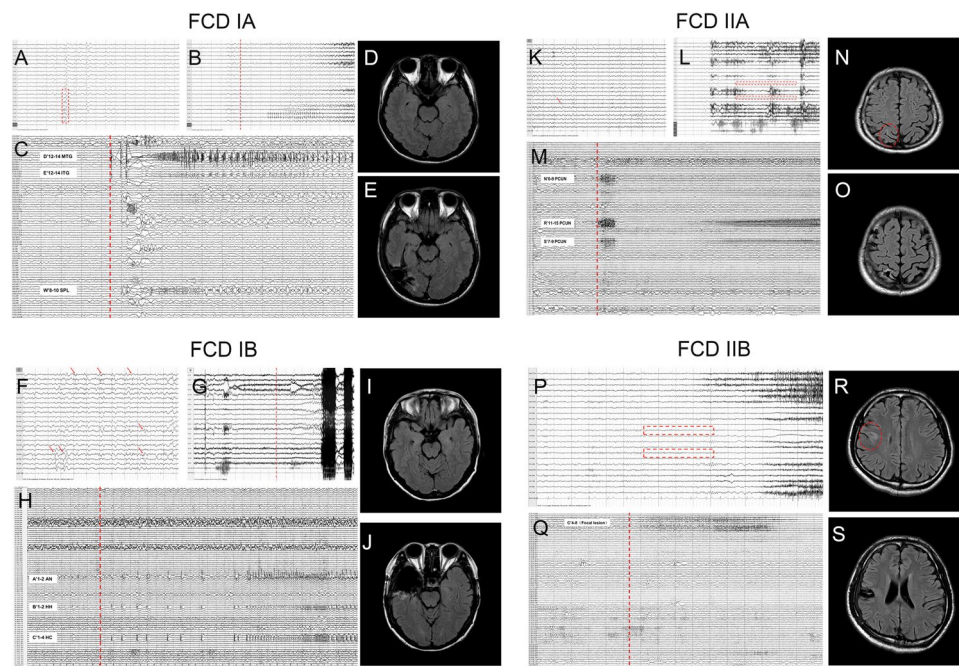
Fig. 1 Representative EEG and MRI results of patients with FCD. **(A-E)** Representative EEG and MRI results of a patient with FCD IA. **(A)** The interictal epileptic discharges (IEDs) were mainly located in the right temporal lobe, accompanied by diffuse, low-amplitude and multiple spike-and-wave discharges. **(B)** The ictal EEG indicated decreased potential in the right hemisphere and rhythmic discharges of 5Hz in the right temporal lobe. **(C)** The ictal SEEG suggested that seizure onset was located at the middle temporal gyrus (MTG) (D'12-14), the inferior temporal gyrus (ITG) (E'12-14), and the superior parietal lobule (SPL) (W'8-10). **(D)** Preoperative MRI showed no obvious lesions. The epileptic focus was located at the cortex of the right temporo-occipital junction. Postoperative MRI was shown in figure **(E)**. **(F-J)** Representative EEG and MRI results of a patient with FCD IB. **(F)** The IEDs showed multiple spike-and-wave discharges in bilateral temporal lobes, spreading to the bifrontal lobes. **(G)** EEG during early ictal period indicated rhythmic discharges of 6Hz in the right hemisphere. **(H)** The ictal SEEG showed that seizure onset was located at the right amygdala nucleus (AN) (A'1-2), hippocampus head (HH) (B'1-2), and hippocampal cauda (HC) (C'1-4).

(I) Preoperative MRI showed no obvious lesions. The epileptic focus was located in the right temporal lobe, and the postoperative MRI was shown in Figure **(J)**. **(K-O)** Representative EEG and MRI results of a patient with FCD IIA. **(K)** The IEDs indicated periodic multiple spike-and-wave discharges in the right central and parietal regions. **(L)** The ictal EEG indicated low-potential and high-frequency discharges in the right central and middle regions. **(M)** The ictal SEEG suggested that the seizure onset was located at the right precuneus (PCUN) (N'6-9; R'11-15; S'7-9). **(N)** Preoperative MRI showed abnormal signals at the right parietal lobe. The epileptic focus was located in the right parietal lobe, and the postoperative MRI was shown in Figure **(O)**. **(P-S)** Representative EEG and MRI results of a patient with FCD IIB. No IEDs was observed in this patient. **(P)** The ictal EEG showed low-voltage fast activity at the right frontal, central, and midline regions. **(Q)** The ictal SEEG suggested that the seizure onset was located at the center of focal dysplasia lesion (C'4-8). **(R)** Preoperative MRI indicated abnormal signals at the right frontal lobe, and the epileptic focus was located in the right frontal lobe. The postoperative MRI was shown in figure **(S)**.

for hematoxylin and eosin staining, as well as for immunohistochemistry for the neuronal marker NeuN, the astroglial marker glial fibrillary acidic protein (GFAP), ADK, adenosine deaminase (ADA), CD73, $A_{2A}R$, mTOR, and GLT-1 as described below. For Western blot analysis, brain tissue from FCD patients (n=4 of each subtype) and surgical controls (n=4) was snap frozen in liquid nitrogen and stored at −80°C until further use.

Immunohistochemistry

Antibodies against ADK (polyclonal rabbit, 1:500; provided by Professor Detlev Boison) [13, 14], ADA (polyclonal rabbit, ab175310, 1:50, Abcam), CD73 (monoclonal mouse, ab91086, 1:50, Abcam), $A_{2A}R$ (polyclonal rabbit, ab79714,

1:100, Abcam), mTOR (monoclonal mouse, SAB2702296, 1:50, Sigma), GLT-1 (polyclonal rabbit, ab41621, 1:100, Abcam), GFAP (monoclonal mouse, DAKO; Glostrup, Denmark, 1:4000), Iba-1 (monoclonal mouse, ab15690, 1:300, Abcam) and NeuN (mouse clone MAB377, IgG1; Chemicon, Temecula, CA; 1:2000) were used for immunohistochemical analysis. Double immunohistochemistry was performed as described previously [13, 27, 33]. After incubation with primary antibodies, sections were incubated for 2 h at room temperature with Alexa Fluor 568- or Alexa Fluor 488-conjugated anti-rabbit IgG labelled with fluorophores in the immunofluorescence, or anti-mouse IgG (1:200; Molecular Probes, Eugene, OR) labelled with peroxidase in the 3-3' diaminobenzidine (DAB) staining. Images were taken using a Leica microscope at Ex/Em wavelengths

of 500/550 nm (green) with an Optronics DEI-750 three-chip camera equipped with a BQ 8000 sVGA frame grabber and analyzed using Bioquant software (Nashville, TN).

Semiquantitative quantification of immunohistochemical staining was performed following our previously published procedures with modifications [14, 16, 30, 43]. The immunoreactivity of each marker in DAB-stained slices was imaged, and a 2x3 mm^2 field was delineated for quantitative analysis using a Kodak imaging device. The immunoreactivity levels were initially quantified in arbitrary units and are expressed as the percent change relative to the internal control (the average immunoreactivity level in the 6 controls). In the FCD type IIB group, the numbers of different types of dysmorphic enlarged neurons and BCs (exhibiting different localization patterns of ADK/A_{2A}R) were determined in a defined area of the lesion (434×326 µm^2).

Western blot analysis

Western blotting and related analysis were performed as described previously with modifications [13, 33]. Freshly frozen histologically normal cerebral cortex samples from surgical controls and cerebral cortex samples from FCD patients (n=4 per group) were homogenized in lysis buffer containing 10 mM Tris (pH 8.0), 150 mM NaCl, 10% glycerol, 1% NP-40, Na-orthovanadate (10.4 mg/ml), 5 mM EDTA (pH 8.0), 5 mM NaF and protease inhibitor cocktail (Boehringer Mannheim, Germany). The protein content was determined using the bicinchoninic acid method. For electrophoresis, equal amounts of proteins (30 µg/lane) were separated by sodium dodecyl sulfate−polyacrylamide gel electrophoresis (SDS−PAGE). The separated proteins were transferred to nitrocellulose membranes for 1.5 h using a semidry electroblotting system (Bio-Rad, Transblot SD, Hercules, CA, USA). The blots were incubated overnight in TTBS (20 mM Tris, 150 mM NaCl, 0.1% Tween, pH 7.5)/5% nonfat dry milk containing an ADK primary antibody (polyclonal rabbit, 1:500; provided by Professor Detlev Boison) [13, 14] or A_{2A}R primary antibody (polyclonal rabbit, ab79714, 1:100, Abcam). After three washes in TTBS, the membranes were incubated in TTBS/5% nonfat dry milk/1% BSA containing goat anti-rabbit or goat anti-mouse antibodies coupled to horseradish peroxidase (1:2500; Dako, Denmark) for 1 h. After three washes in TTBS, immunoreactivity was visualized using Lumi–Light PLUS Western Blotting Substrate (Roche Diagnostics, Mannheim, Germany), and images were digitized using a Luminescent Image Analyzer (LAS-3000, Fuji Film, Japan). The density of β-actin (monoclonal mouse antibody, Sigma, St. Louis, MO, USA 1:50.000) was used as a reference. The levels of ADK and A_{2A}R were normalized to internal standards and are expressed relative to the level in the control group.

Statistical analysis

Statistical analyses were performed with SPSS for Windows (SPSS 11.5, SPSS Inc., Chicago, IL, USA) using unpaired two-tailed t tests. P <0.05 was considered significant.

Results

The histopathological features of different types of FCD

Normal-appearing neocortical samples exhibited a layered structure typical of the human neocortex (Fig. 2A, F). In contrast, marked cortical dyslamination was seen in FCD lesions. FCD type IA lesions were characterized by abnormal radial cortical lamination (Fig. 2B, G), and FCD types IB lesions usually exhibited abnormal tangential cortical lamination (Fig. 2C, H). The hallmark of FCD type IIA (Fig. 2D, I) was the presence of dysmorphic neurons (Fig. 2I, arrow), which exhibited a significantly enlarged cell body and nucleus, malorientation, abnormally distributed intracellular Nissl substance, and cytoplasmic accumulation of neurofilament proteins. There were no BCs detected in FCD type IIA sections by immunohistochemistry. The hallmark of FCD type IIB lesions (Fig. 2E, J) was the presence of dysmorphic enlarged neurons (Fig. 2J, arrow) and BCs (Fig. 2J, arrowheads). BCs usually exhibited a large cell body, eccentric nucleus and glassy eosinophilic cytoplasm (Fig. 2J, arrowheads).

In addition, astrogliosis was also observed in FCD type I and type II specimens. Sections of cortical gray matter and white matter from surgical specimens from the control and FCD groups were subjected to immunochemistry GFAP (Fig. 3). In control specimens, sparse GFAP density in astrocytes was detected in the white matter (Fig. 3A1-A3). Within FCD type IA (Fig. 3B1-B3), FCD type IB (Fig. 3C1-C3), FCD type IIA (Fig. 3D1-D3), and FCD type IIB (Fig. 3E1-E3) lesions, astrogliosis was observed in both the gray matter and white matter. Reactive astrocytes were also usually hypertrophic (B3, C3, D3, arrows). Of note, GFAP-positive dysmorphic enlarged neurons (E2, E3, arrows) and GFAP-positive BCs (E2, E3, arrowheads) were also detected in FCD type IIB specimens.

Dysregulation of adenosine signaling in FCD

Increased density of ADK in FCD

As an enzyme with high affinity and low capacity, ADK is the major adenosine-metabolizing enzyme under baseline conditions[44, 45]. Adenosine deficiency caused
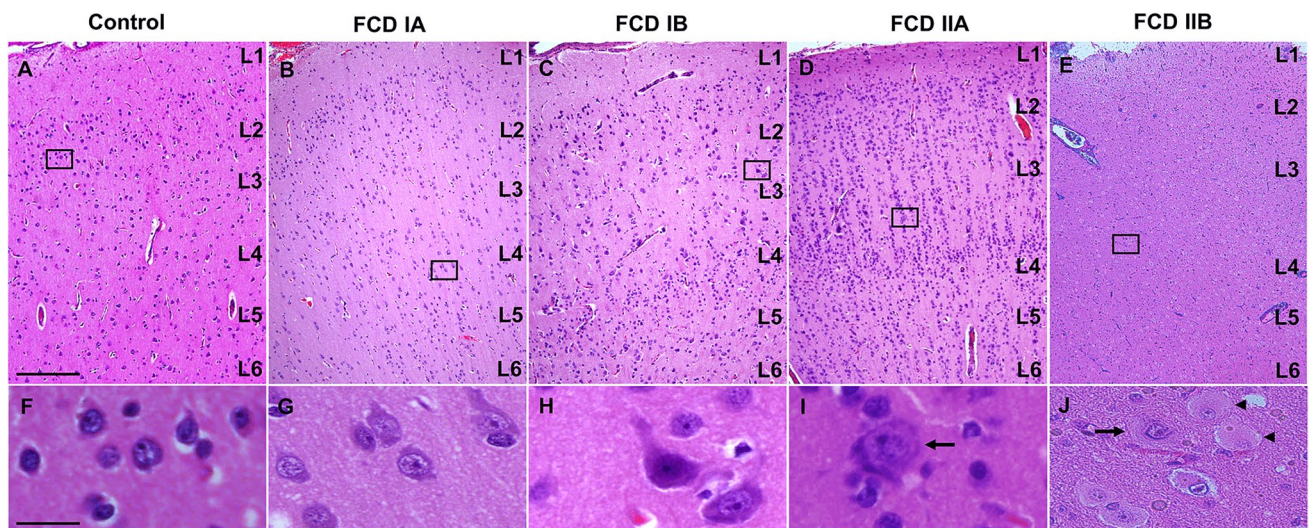
Fig.2 Characteristic neuropathological findings in brain tissue from different types of human FCD. **(A, F)** Normal appearing neocortex with characteristic layers L1–L6. **(B, G)** Histopathological findings in FCD IA (abnormal radial lamination and abundant microcolumns). Distinct microcolumnar arrangements of small diameter neurons are detected in FCD IA specimen cut perpendicular to the pial surface. **(C, H)** Histopathological findings in FCD IB (abnormal tangential layer composition). Failure to establish a six-layered tangential composition of the neocortex is a hallmark of this variant. **(D, I)** Histopathological findings in FCD IIA. **(D)** Microscopic inspection of surgical specimen reveals severe cortical dyslamination without the formation of distinguishable layers (except layer 1). **(I)** High-power magnification of dysmorphic enlarged neurons with significantly enlarged cell body and nucleus **(arrow)**. No balloon cells are identified. **(E, J)** Histopathologic findings in FCD IIB. **(E)** Severe cortical dyslamination (except layer 1) and increased cortical thickness. **(J)** The hallmark of FCD IIB is the presence of dysmorphic enlarged neurons **(arrow)** and balloon cells **(arrowheads)**. Balloon cells usually present with eccentric nucleus, enlarged pale and opalescent glassy eosinophilic cytoplasm **(J, arrowheads)**. All sections are H&E stained on 4μm paraffin embedded specimens. Scale bars=(A-E) 500μm; (F-J) 15μm.

by increased level of ADK is sufficient to induce spontaneous and recurrent epileptic seizures[19]. Here, we studied the density and localization of ADK in resected tissue from FCD patients and control subjects by immunohistochemistry. Consistent with previous findings of low density of ADK in the normal cerebral cortex[13], we found only negative or weak ADK immunoreactivity in the gray (Fig. 4 A1-A2) and white (Fig. 4 A3) matter in control samples. In contrast, we observed increased ADK immunoreactivity in specimens from patients with FCD type IA (Fig. 4 B1-B3), type IB (Fig. 4 C1-C3), type IIA (Fig. 4 D1-D3) and type IIB (Fig. 4 E1-E3), which exhibited (I) globally (in neurons and astrocytes) increased density of ADK and (II) ectopic localization of ADK in the cell nucleus (D3, arrowhead). In samples from FCD type I patients, ADK was predominantly located in the cytoplasm of cortical neurons (Figure 4 B2, C2, arrows). In the white matter of samples from FCD type I patients, strong ADK immunoreactivity was observed in hypertrophic astrocytes (Fig. 4B3, C3, arrows). In addition, a large amount of ADK was located in the cytoplasm of dysmorphic enlarged neurons in FCD type IIA (Fig. 4D2, D3, arrows) and FCD type IIB (Fig. 4E2, E3, arrows) specimens, as well as in the cytoplasm of BCs in FCD type IIB (Fig. 4E3, arrowhead) specimens. Interestingly,

we also observed ectopic localization of ADK in the nuclei of dysmorphic enlarged neurons in FCD type IIA specimens (Fig. 4D3, arrowhead). Both immunohistochemistry (Fig. 4F, G) and Western blot analysis (Fig. 9A, B(revealed a significant increase in ADK density in all FCD subgroups compared to the control group.

Notably, the results of immunohistochemistry and double labeling revealed four distinct localization patterns of ADK in dysmorphic enlarged neurons and BCs in FCD type IIB specimens (Fig. 5). There were dysmorphic enlarged neurons and BCs not expressing ADK (11.56%±3.60% and 17.55%±2.70% of all cells, respectively), those with ADK localization only in the cytoplasm (79.90%±6.16% and 77.34%±3.28% of all cells, respectively), those with ADK localization only in the nucleus (6.29%±2.64% and 3.79±3.38% of all cells, respectively), and those with ADK localization in both the cytoplasm and nucleus (2.25%±1.93% and 1.32%±1.07% of all cells, respectively) (Fig. 5).

Increased density of ADA in FCD

ADA is a low-affinity, high-capacity enzyme involved in the metabolic clearance of adenosine under conditions of adenosine overload. Immunohistochemistry for ADA revealed
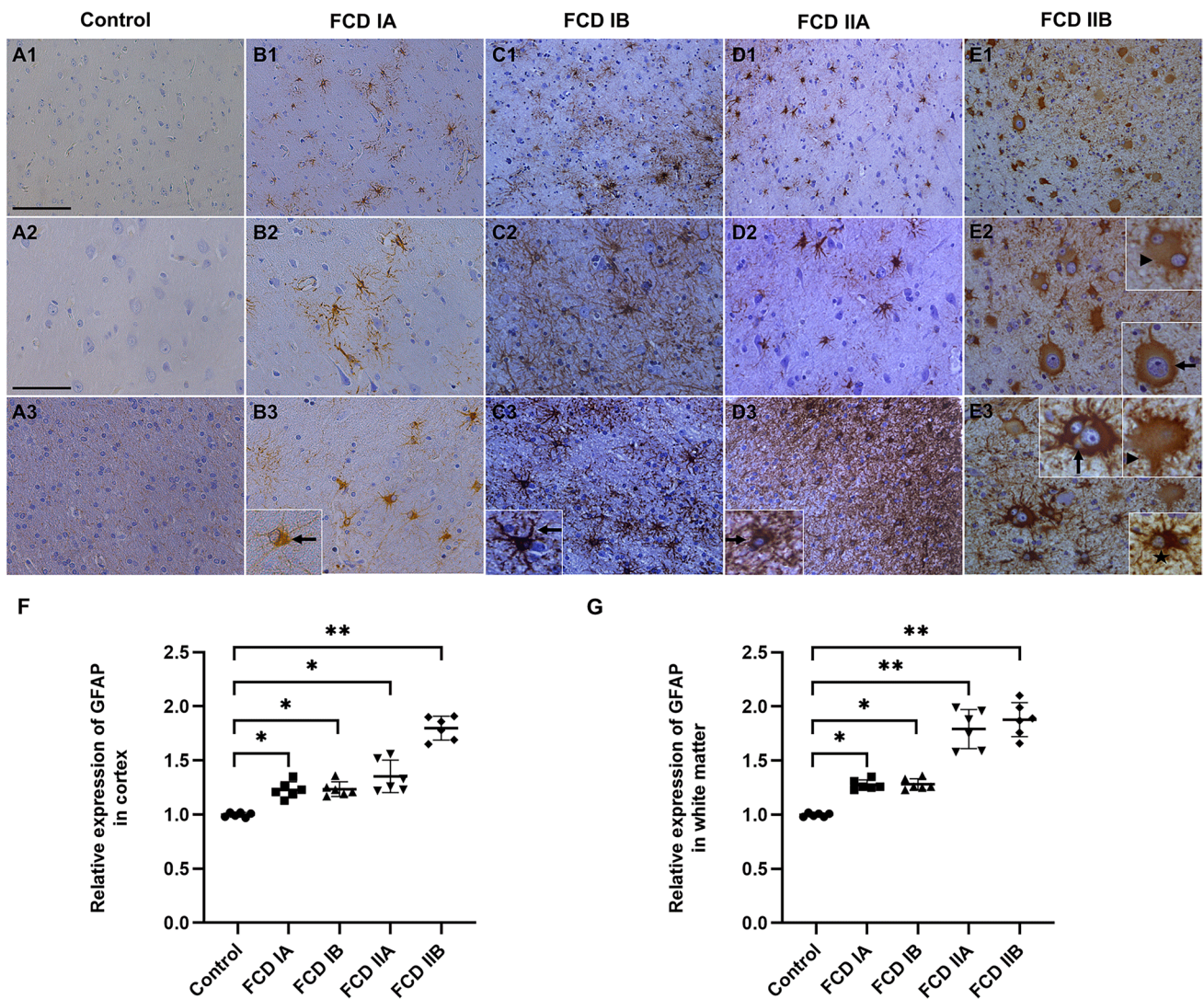
Fig. 3 Density and localization of GFAP within the lesions of different types of FCD. **(A1-A3)** Weak immunostaining for GFAP in control cortical gray matter **(A1, A2)** and white matter **(A3)**. **(B1-B3, C1-C3, D1-D3)** Reactive astrogliosis in cortical gray matter within the lesions of FCD IA **(B1, B2)**, FCD IB **(C1, C2)**, FCD IIA **(D1, D2),** and white matter within the lesions of FCD IA **(B3)**, FCD IB **(C3)** and FCD IIA **(D3)**. Reactive astrocytes are usually accompanied by hypertrophied morphologic variations **(B3, C3, D3, arrows)**. **(E1-E3)** In the gray **(E1-E2)** and white matter **(E3)** within the lesions of FCD IIB, we detect GFAP-positive dysmorphic enlarged neurons

(E2, E3, arrows), GFAP-positive balloon cells (BCs) with binucleation **(E2, arrowhead)**, GFAP-positive BCs without apparent nuclei **(E3, arrowhead)**, and GFAP-positive astrocytes **(E3, star)**. Scale bars= **(A1, B1, C1, D1, E1)** 100µm; **(A2-A3, B2-B3, C2-C3, D2-D3, E2-E3)** 50µm. **(F-G)** Semiquantitative analysis of scanned immunodensities shows a significant increase of GFAP density in both the cortex **(F)** and the white matter **(G)** of FCD compared with controls (n=6 in each group; *: $P<0.05$, **: $P<0.01$; Statistical analyses were made using unpaired two-tailed t-test; Individual data points were plotted, with error bars ± SD).

sparse ADA density in astrocytes in the cortical gray matter (Fig. 6A1-A2) and white matter (Fig. 6A3) of control specimens. Importantly, we observed increased density of ADA in specimens from patients with FCD type IA (Fig. 6B1-B3), type IB (Fig. 6C1-C3), type IIA (Fig. 6D1-D3) and type IIB (Fig. 6E1-E3), which exhibited increased density of ADA in hypertrophied astrocytes in white matter within FCD lesions (Fig. 6B3, C3, arrows; D3, arrowhead; E3, star). Specifically, within the gray matter of FCD type IA (Fig. 6B2, arrow) and FCD type IB (Fig. 6C2, arrow) specimens, there was no

ADA localized in neurons. In addition, marked cytoplasmic staining of ADA was found in dysmorphic enlarged neurons in FCD type IIA (Fig. 6D2, D3, arrows) and FCD type IIB (Fig. 6E2, E3, arrows) specimens. In addition, we detected ectopic perinuclear localization of ADA in BCs in FCD type IIB specimens (Fig. 6E3, arrowhead). Semiquantitative analysis of immunoreactivity revealed a significant increase in ADA immunoreactivity in the white matter in FCD specimens compared to control specimens (n=6 in each group) (Fig. 6F, G).
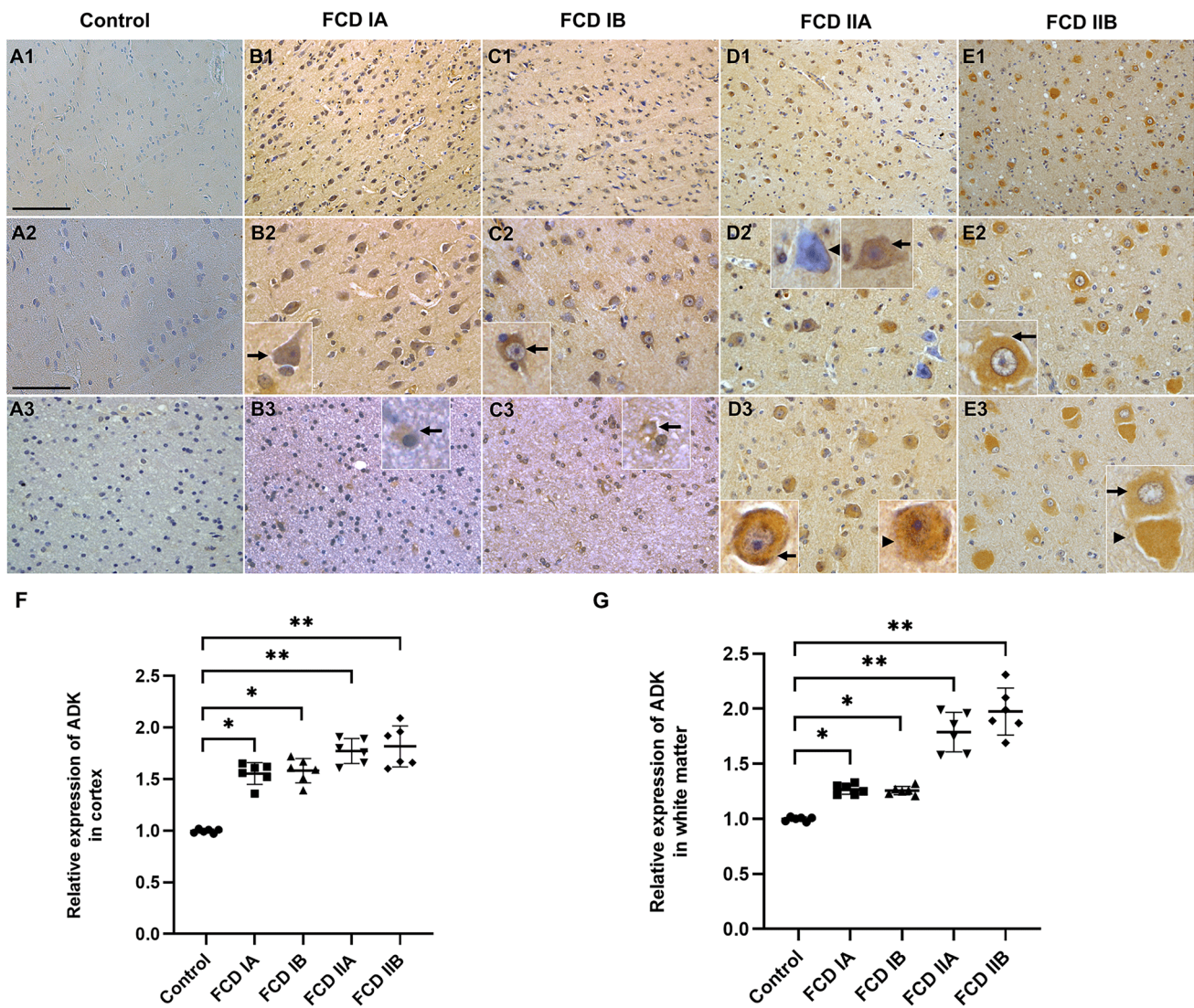
Fig. 4 Density and localization of ADK within the lesions of different types of FCD. **(A1-A3)** Negative or weak immunostaining for ADK in control cortical gray matter **(A1, A2)** and white matter **(A3)**. **(B1-B3, C1-C3)** Within the lesions of FCD IA **(B1-B3)** and FCD IB **(C1-C3)**, we detect cytoplasmic localization of ADK in cells with neuronal morphology in gray matter **(B1, C1; B2, C2, arrows)** and in cells with morphology of ectopic neurons **(B3, arrow)** as well as reactive astrocytes **(C3, arrow)** in white matter. **(D1-D3)** In the gray matter **(D1-D2)** and white matter **(D3)** within the lesion of FCD IIA, we detect cytoplasmic localization **(D2, D3, arrows)** and also both cytoplasmic and nuclear localization **(D3, arrowhead)** of ADK in dysmorphic enlarged neurons. There are also some dysmor-phic enlarged neurons without ADK localization **(D2, arrowhead)**. **(E1-E3)** In the gray matter **(E1-E2)** and white matter **(E3)** within the lesions of FCD IIB, we detect cytoplasmic localization of ADK in dysmorphic enlarged neurons **(E2, E3, arrows)** and balloon cells **(E3, arrowhead)**. Scale bars= **(A1, B1, C1, D1, E1)** 100μm; **(A2-A3, B2-B3, C2-C3, D2-D3, E2-E3)** 50μm. **(F-G)** Semiquantitative analysis of scanned immunodensities demonstrates a significant increase of ADK density in both the cortex **(F)** and the white matter **(G)** of FCD compared with controls ($n=6$ in each group; *: $P<0.05$, **: $P<0.01$; Statistical analyses were made by unpaired two-tailed t-test; Individual data points were plotted, with error bars $\pm$ SD).

Increased density of CD73 in FCD

CD73 is the enzyme that generates adenosine from extracellular adenine nucleotides. Concomitant increased level of CD73 and $A_{2A}R$ has been found in specimens from patients with epilepsy associated with RE [27]. In the present study, increased level of CD73 was found in both the gray matter and white matter in specimens from FCD patients (Fig. 7).

In contrast, weak or negative CD73 immunoreactivity was observed in the gray and white matter of control specimens (Fig. 7A1-A3). Specifically, within the gray matter of FCD type I specimens, CD73 immunoreactivity was detected in neurons (Fig. 7B2, C2, arrows). In the white matter of FCD type I and type II specimens, CD73 immunoreactivity was observed in hypertrophied astrocytes (Fig. 7B3, C3 D3, E3, arrows). In addition, increased level of CD73 was found in

dysmorphic enlarged neurons in FCD type IIA (Fig. 7D2, arrowhead) and FCD type IIB specimens (Fig. 7E2, arrowhead), as well as in BCs in FCD type IIB specimens (Fig. 7 E3, arrowhead). Semiquantitative analysis of immunoreactivity revealed a significant increase in CD73 immunoreactivity in FCD specimens compared to control specimens ($n=6$ in each group) (Fig. 7F, G).

Increased density of $A_{2A}R$ in FCD

Consistent with previous studies [27], we found negative or weak $A_{2A}R$ density in control specimens (cortical gray matter, Fig. 8A1-A2; white matter, Fig. 8A3). In contrast, we observed increased level of $A_{2A}R$ in FCD type IA (Fig. 8B1-B3), type IB (Fig. 8C1-C3), type IIA (Fig. 8D1-D3) and type IIB (Fig. 8E1-E3) specimens, which exhibited (I) globally (in neurons and astrocytes) increased density of $A_{2A}R$ and (II) localization of $A_{2A}R$ within cells (in the cytoplasm or nucleus). Specifically, in the gray matter of FCD type I specimens, $A_{2A}R$ was predominantly located surrounding the nucleus in cortical neurons (Fig. 8B2, C2, arrows). In the white matter of FCD type I specimens, strong $A_{2A}R$ immunoreactivity was observed in hypertrophied astrocytes (Fig. 8B3, C3, arrows) and ectopic neurons (Fig. 8C3, arrowhead). Marked perinuclear staining of $A_{2A}R$ was also detected in dysmorphic enlarged neurons in FCD type IIA specimens (Fig. 8D2, arrow). In addition, we detected some ectopic localization patterns of $A_{2A}R$ in FCD lesions. On the one hand, $A_{2A}R$ was located in the cytoplasm in dysmorphic enlarged neurons (Fig. 8D3, arrow) in FCD type IIA specimens and in BCs (Fig. 8E3, arrow), dysmorphic enlarged neurons (Fig. 8E2, arrowhead), microglia (Fig. 8E3, circle), and reactive astrocytes (Fig. 8E3, star) in FCD type IIB specimens. On the other hand, $A_{2A}R$ was located in both the cytoplasm and nucleus in dysmorphic enlarged neurons (Fig. 8E2, arrow) and BCs (Fig. 8E3, arrowhead) in FCD type IIB specimens. Both immunohistochemistry (Fig. 8F, G) and Western blot analysis (Fig. 9A, D) revealed a significant increase in $A_{2A}R$ density in the FCD group compared to the control group.

Double staining for $A_{2A}R$ and GFAP and Iba-1 and NeuN demonstrated different ectopic patterns of $A_{2A}R$ localization in astrocytes, microglia, and neurons, as well as in dysmorphic enlarged neurons and BCs within FCD type IIB lesions (Fig. 10). In GFAP-positive astrocytes within FCD type IIB lesions (Fig. 10A4, B4), as well as in reactive astrocytes surrounding BCs (Fig. 10D4, arrowhead), nuclear localization (Fig. 10A4, B4, arrows; D4, arrowhead) and cytoplasmic localization (Fig. 10A4, arrowhead) of $A_{2A}R$ were found. The findings revealed two distinct subtypes of astrocytes: astrocytes with nuclear but not cytoplasmic $A_{2A}R$ localization and astrocytes with cytoplasmic but not nuclear $A_{2A}R$ localization. In Iba-1-positive microglia,

cytoplasmic localization of $A_{2A}R$ was found (Fig. 10G4, arrow). In NeuN-positive neurons, perinuclear localization of $A_{2A}R$ was observed (Fig. 10H4, arrowhead). In addition, we detected $A_{2A}R$ density in dysmorphic enlarged neurons and BCs. Nuclear localization of $A_{2A}R$ was found in GFAP-negative BCs (Fig. 10D4, E4, arrows), GFAP-positive BCs (Fig. 10F4, arrow), NeuN-positive BCs (Fig. 10H4, arrow), GFAP-positive dysmorphic enlarged neurons (Fig. 10C4, arrow) and GFAP-negative dysmorphic enlarged neurons (Fig. 10E4, arrowhead). Nuclear localization of $A_{2A}R$ was found in a small fraction of dysmorphic enlarged neurons ($13.66\%\pm3.61\%$) and BCs ($11.52\%\pm3.00\%$), whereas a large fraction of dysmorphic enlarged neurons ($86.34\%\pm3.61\%$) and BCs ($88.48\%\pm3.00\%$) did not show nuclear localization of $A_{2A}R$.

Reduced density of GLT-1 in FCD

Interactions between $A_{2A}R$ and GLT-1 aggravate glutamate excitotoxicity and promote cell death in patients with RE [27]. This interaction may also constitute the pathological basis of FCD. Based on this hypothesis, we explored the localization patterns of GLT-I in FCD patients. Consistent with previous results [27], we found a patchy distribution of GLT-1 immunoreactivity in the gray matter of control samples; specifically, GLT-1 exhibited a normal localization pattern but was strongly located in glial cell processes (Fig. 11A1, A2). In the white matter of control specimens, only a few GLT-1-expressing astrocytes were found (Fig. 11A3). However, in the gray matter and white matter of FCD type IA (Fig. 11B1-B3), FCD type IB (Fig. 11C1-C3), FCD type IIA (Fig. 11D1-D3) and FCD type IIB (Fig. 11E1-E3) lesions, sparse or no GLT-1 density was observed in astrocytes. Semiquantitative analysis of immunoreactivity revealed a significant decrease in GLT-1 immunoreactivity in the cortex in FCD specimens compared to control specimens ($n=6$ in each group) (Fig. 11F, G).

Increased density of mTOR in FCD

We analyzed mTOR density in brain specimens from FCD patients and surgical controls by immunohistochemistry and found increased level of mTOR in the white matter of FCD type I specimens and in both the white matter and gray matter of FCD type II specimens (Fig. 12). In contrast, weak or negative mTOR immunoreactivity was observed in the gray and white matter of control specimens (Fig. 12A1-A3). In the white matter of FCD type I and II specimens, mTOR immunoreactivity was observed in hypertrophied astrocytes (Fig. 12B3, C3 arrows; D3, arrowhead; E3, star). Within the gray matter of FCD type IA (Fig. 12B2) and FCD type IB (Fig. 12C2) lesions, there was no mTOR immunoreactivity detected in neurons. In addition, increased level of mTOR
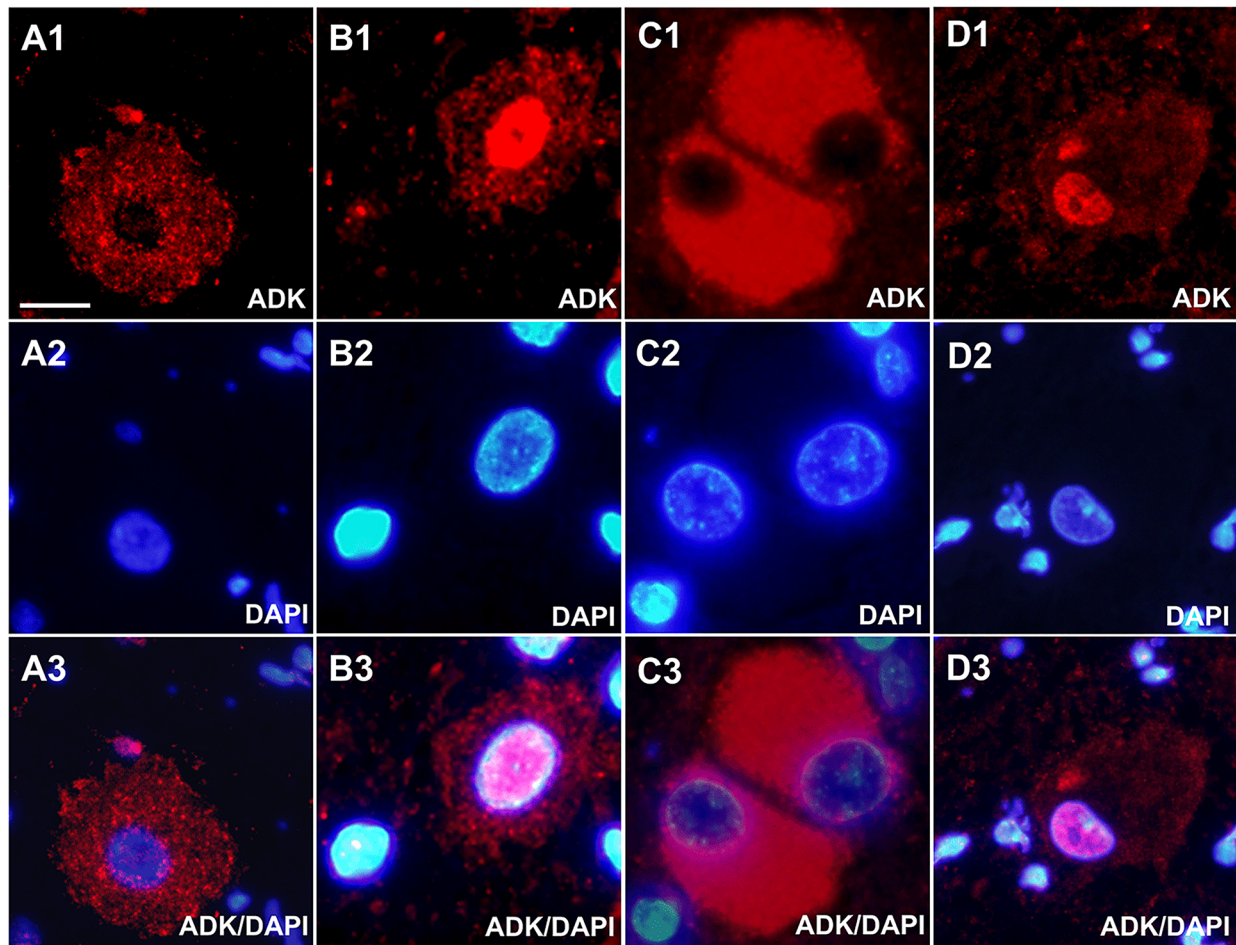
Table. Percentage of different expression patterns of ADK in dysmorphic enlarged neurons/balloon cells.

Dysmorphic enlarged neurons	Range of number	Percentage (mean ± SD)
Total number	30-46	/
ADK negative	3-7	11.56%±3.60%
ADK positive	26-40	88.44%±3.60%
Cytoplasm positive only	25-38	79.90%±6.16%
Nuclear positive only	1-4	6.29%±2.64%
Both nuclear and cytoplasm positive	0-2	2.25%±1.93%
Balloon cells	**Range of number**	**Percentage (mean ± SD)**
Total number	33-61	/
ADK negative	6-12	17.55%±2.70%
ADK positive	26-52	82.45%±2.70%
Cytoplasm positive only	26-49	77.34%±3.28%
Nuclear positive only	0-4	3.79%±3.38%
Both nuclear and cytoplasm positive	0-1	1.32%±1.07%

◄**Fig. 5** Density and localization of ADK within the lesions of FCD IIB. **(A1-A3)** Cytoplasmic localization of ADK in dysmorphic enlarged neurons. **(B1-B3)** Ectopic nuclear localization of ADK in dysmorphic enlarged neurons. **(C1-C3)** Cytoplasmic localization of ADK in balloon cells. **(D1-D3)** Ectopic nuclear localization of ADK in balloon cells. Table in this figure shows the percentage of different localization patterns of ADK in dysmorphic enlarged neurons or balloon cells. **(A1, B1, C1, D1)** ADK (red); **(A2, B2, C2, D2)** DAPI (blue). Scale bar=15μm.

was found in dysmorphic enlarged neurons in FCD type IIA (Fig. 12D2, D3, arrows) and FCD type IIB (Fig. 12E2, E3, arrows) specimens, as well as in BCs in FCD type IIB (Fig. 12E2, E3, arrowheads) specimens. Semiquantitative analysis of immunoreactivity revealed a significant increase in mTOR immunoreactivity in the white matter in FCD type I specimens and in both the white matter and gray matter in FCD type II specimens compared to control specimens (*n*=6 in each group) (Fig. 12F, G).

Colocalization of ADA, ADK and A$_{2A}$R with mTOR in FCD type IIB lesions

Next, we explored whether ADA, ADK and A$_{2A}$R were colocalized with mTOR within FCD type IIB lesions. Double staining for ADA and mTOR indicated that they were colocalized in BCs (Fig. 13A4, arrow) and neurons (Fig. 13A4, arrowheads) within FCD type IIB lesions. Double staining for ADK and mTOR indicated that they were colocalized in BCs (Fig. 13B4, arrow) and astrocytes (Fig. 13B4, arrowhead) within FCD type IIB lesions. Double staining for A$_{2A}$R and mTOR indicated they were colocalized in BCs (Fig. 13C4, arrow) and astrocytes (Fig. 13C4, arrowhead) within FCD type IIB lesions.

Discussion

FCD is a developmental malformation of the cerebral cortex that is associated with the development of pharmacoresistant epilepsy. FCD patients usually present with seizures in early childhood, and some also exhibit other clinical manifestations, including cognitive impairment, developmental delay, behavioral disorders, autism spectrum disorders, and focal neurological deficits [1]. Seizure origin and the occurrence of additional clinical symptoms are determined by the anatomical location of FCD, which can be detected by MRI or histopathological examination of resected tissue specimens. Although the pathogenesis of FCD remains to be defined, the association between the adenosine system and FCD-associated epilepsy was suggested by our previous study [13]. Adenosine is an endogenous anticonvulsant and acts as a seizure terminator in the brain [19]. Our previous data indicated that increased level of ADK and consequent adenosine deficiency in FCD lesions are strongly associated with the development of pharmacoresistant epilepsy [13]. In this study, through immunohistochemistry and Western blot analysis, we first evaluated maladaptive changes in the adenosine system within FCD type I and type II lesions and found increased density of the two major adenosine-metabolizing enzymes ADK and ADA, as well as the major adenosine-producing enzyme CD73, suggesting increased turnover of adenosine. We also found an increase in A$_{2A}$R density in conjunction with alterations in two pathways interacting with A$_{2A}$R, as shown by a decrease in the density of the astroglial glutamate transporter GLT-1 and increased density of mTOR. These results suggest that dysregulation of the adenosine system and its downstream pathways is a common pathological feature of FCD. Adenosine-metabolizing enzymes or adenosine receptors might therefore be considered potential targets for the treatment of epilepsy associated with FCD.

Adenosine is a ubiquitous inhibitory modulator released during seizures and has been shown to mediate seizure arrest, postictal refractoriness, and suppression of epileptogenesis [19]. Neuronal excitability in the brain is modulated by activation of G protein-coupled adenosine receptors, specifically inhibitory A$_1$Rs and facilitatory A$_{2A}$Rs [18]. The equilibrium of adenosine receptor density levels, as well as the availability of endogenous adenosine to activate the receptors, plays a crucial role in the development and progression of epilepsy [18]. In both epilepsy patients and animal models, adenosine dysfunction, including upregulation of the major adenosine-metabolizing enzyme ADK, subsequent reduction in adenosine tone [13-15], and increased density of A$_{2A}$Rs [27], has been demonstrated to promote epileptogenesis and seizures [46].

Astrocytic ADK is the major adenosine-metabolizing enzyme in the brain. Extracellular levels of adenosine are regulated mainly by an astrocyte-based adenosine cycle, with astrocytes serving as the key metabolic sink for adenosine through its clearance via ADK [47]. In line with this role, genetic disruption of ADK density increases extracellular adenosine levels [48]. Upregulation of ADK and the consequent reduction in extracellular adenosine concentrations are sufficient to induce seizures through insufficient activation of A$_1$Rs [14, 49]. Thus, increased level of ADK in conjunction with astrogliosis has been demonstrated to be a pathological hallmark of experimental epilepsy as well as temporal lobe epilepsy, RE, and tumor-associated epilepsy [31, 33, 50]. In the present study, we found robust increased level of ADK in reactive astrocytes and neurons within FCD type I lesions, as well as in dysmorphic enlarged neurons and BCs in FCD type II lesions. These results indicate that increased level of astrocytic ADK might play a role in epileptogenesis in FCD patients.
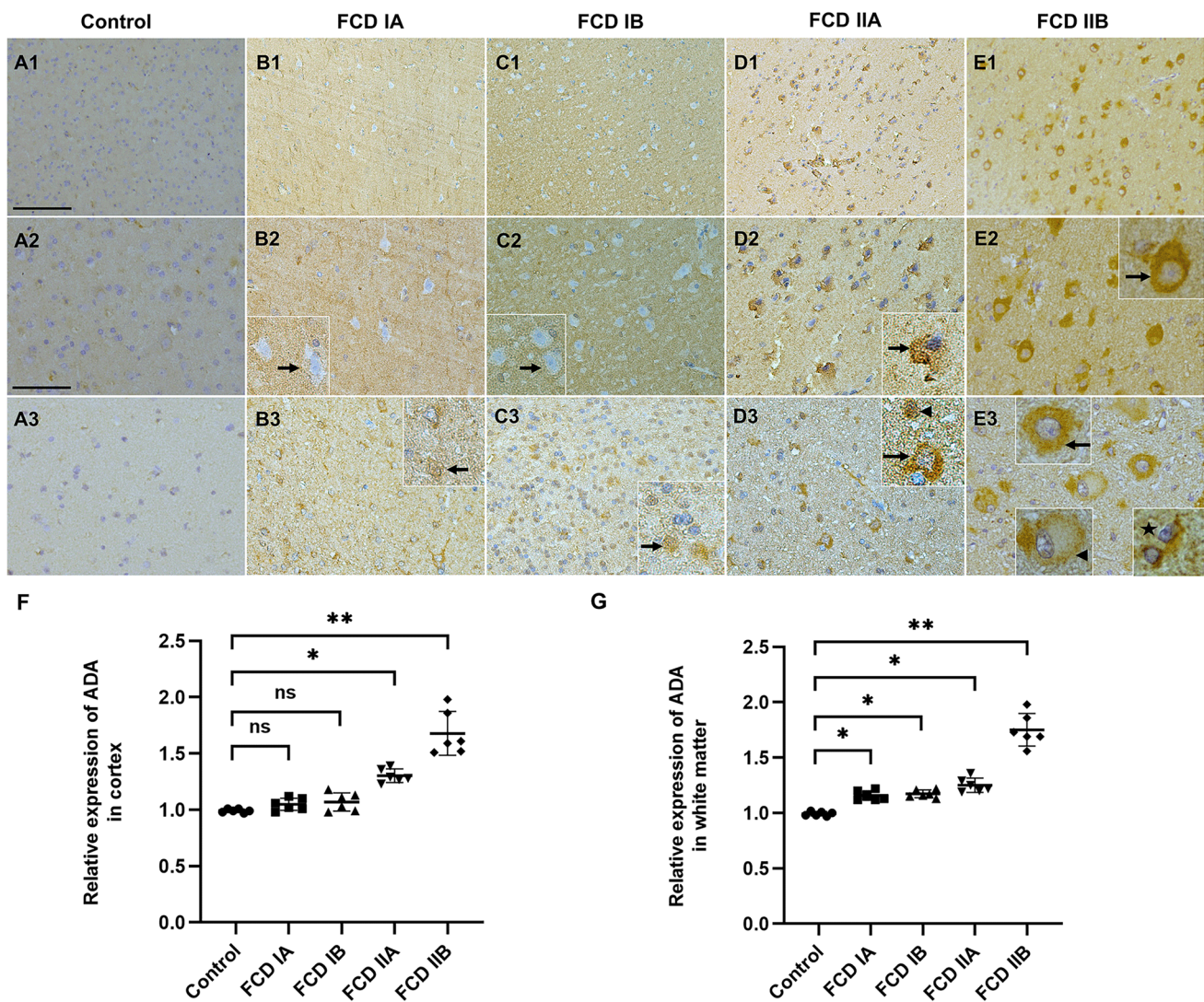
Fig. 6 Density and localization of ADA within the lesions of different types of FCD. **(A1-A3)** Sparse density of ADA in cells with astrocyte morphology in control cortical gray matter **(A1-A2)** and white matter **(A3)**. **(B1-B3, C1-C3)** Within the lesions of FCD IA **(B1-B3)** and FCD IB **(C1-C3)**, we find a lack of ADA density in cells with neuronal morphology in the gray matter **(B1, C1; B2, C2, arrows)** and predominate cytoplasmic localization of ADA in cells with morphology of reactive astrocytes in the white matter **(B3, C3, arrows)**. **(D1-D3)** In the gray matter **(D1-D2)** and white matter **(D3)** within the lesions of FCD IIA, we find cytoplasmic localization of ADA in dysmorphic enlarged neurons **(D2, D3, arrows)** and in cells with the morphology of reactive astrocytes **(D3, arrowhead)**. **(E1-E3)** In the gray matter **(E1-E2)** and white matter **(E3)** within the lesions of FCD IIB, we find cytoplasmic localization of ADA in dysmorphic enlarged neurons **(E2, E3, arrows)** and cells with the morphology of reactive astrocytes **(E3, star)**. We also find ectopic perinuclear localization of ADA in the balloon cells in the white matter **(E3, arrowhead)**. Scale bars= **(A1, B1, C1, D1, E1)** 100μm; **(A2-A3, B2-B3, C2-C3, D2-D3, E2-E3)** 50μm. **(F-G)** Semiquantitative analysis of immunodensities demonstrates a significant increase of ADA density in the cortex **(F)** of FCD type II, and in the white matter **(G)** of both FCD type I and II compared with controls ($n=6$ in each group; *: $P<0.05$, **: $P<0.01$, ns: no significance; Statistical analyses were made using unpaired two-tailed t-test; Individual data points were plotted, with error bars $\pm$ SD).

There are two alternatively spliced forms of ADK: ADK-long (ADK-L), which is located in the nucleus, and ADK-short (ADK-S), which is located in the cytoplasm [51]. Cytoplasmic ADK-S determines intra- and extracellular levels of adenosine, which are balanced through equilibrative nucleoside transporters. Therefore, intracellular ADK-S determines the activation of adenosine receptors and thereby contributes to the regulation of neuronal excitability [36, 52]. ADK-L is localized in the nucleus and is needed to maintain methylation reactions, including DNA and histone methylation, which play a role in the regulation of epileptogenesis and cell proliferation [19]. Increased level of both subtypes of ADK was detected within FCD lesions in the present study. These results suggest that
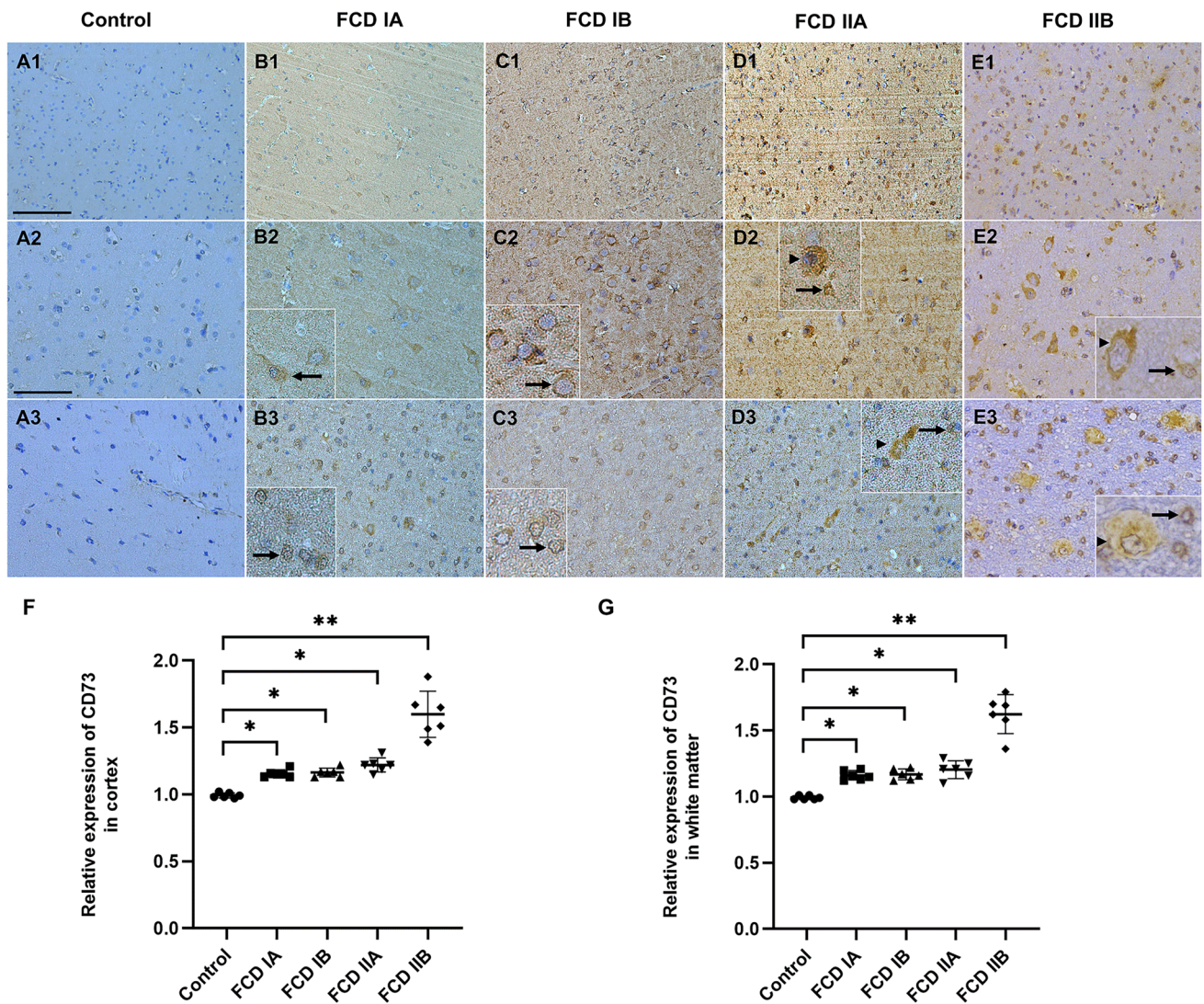
Fig. 7 Density and localization of CD73 within the lesions of different types of FCD. (**A1-A3**) Negative or weak density of CD73 in the control cortical gray matter (**A1-A2**) and the control white matter (**A3**). (**B1-B3, C1-C3**) Within the lesions of FCD IA (**B1-B3**) and FCD IB (**C1-C3**), we detect cytoplasmic localization (**B2, arrow**) and perinuclear localization (**C2, arrow**) of CD73 in cells with neuronal morphology in the gray matter, and cytoplasmic localization in cells with morphology of reactive astrocytes in the white matter (**B3, C3, arrows**). (**D1-D3**) In the gray matter (**D1-D2**) and white matter (**D3**) within the lesions of FCD IIA, we detect cytoplasmic localization of CD73 in dysmorphic enlarged neurons (**D2, arrowhead**), cells with neuronal morphology (**D3, arrowhead**) and cells with morphology of reactive astrocytes (**D2, D3, arrows**). (**E1-E3**) In the gray (**E1-E2**) and white matter (**E3**) within the lesions of FCD IIB, we find cytoplasmic localization of CD73 in balloon cells (**E3, arrowhead**) and in cells with morphology of reactive astrocytes (**E2, E3, arrows**). We also find the perinuclear localization of CD73 in dysmorphic enlarged neurons (**E2, arrowhead**). Scale bars= (**A1, B1, C1, D1, E1**) 100μm; (**A2-A3, B2-B3, C2-C3, D2-D3, E2-E3**) 50μm. (**F-G**) Semiquantitative analysis of immunodensities demonstrates a significant increase of CD73 density in both the cortex (**F**) and the white matter (**G**) of FCD compared with controls (n=6 in each group; *: $P<0.05$, **: $P<0.01$; Statistical analyses were made using unpaired two-tailed t-test; Individual data points were plotted, with error bars ± SD).

dysregulation of ADK density may impact FCD on different levels: the increase in ADK-L levels may drive epileptogenesis through an epigenetic mechanism and may affect cell proliferation during cortical development, whereas the increase in ADK-S levels may directly decrease seizure thresholds through insufficient activation of A_1Rs and thereby contribute to seizures in FCD.

In addition to the increased level of ADK in astrocytes, we found ectopic localization of both isoforms of ADK in neurons and BCs within FCD type I and type II lesions. Developmental studies performed in mice suggest that there is a switch in the ADK localization pattern in the brain from neuronal localization during the perinatal period to nearly exclusive astrocytic localization in adulthood, suggesting an
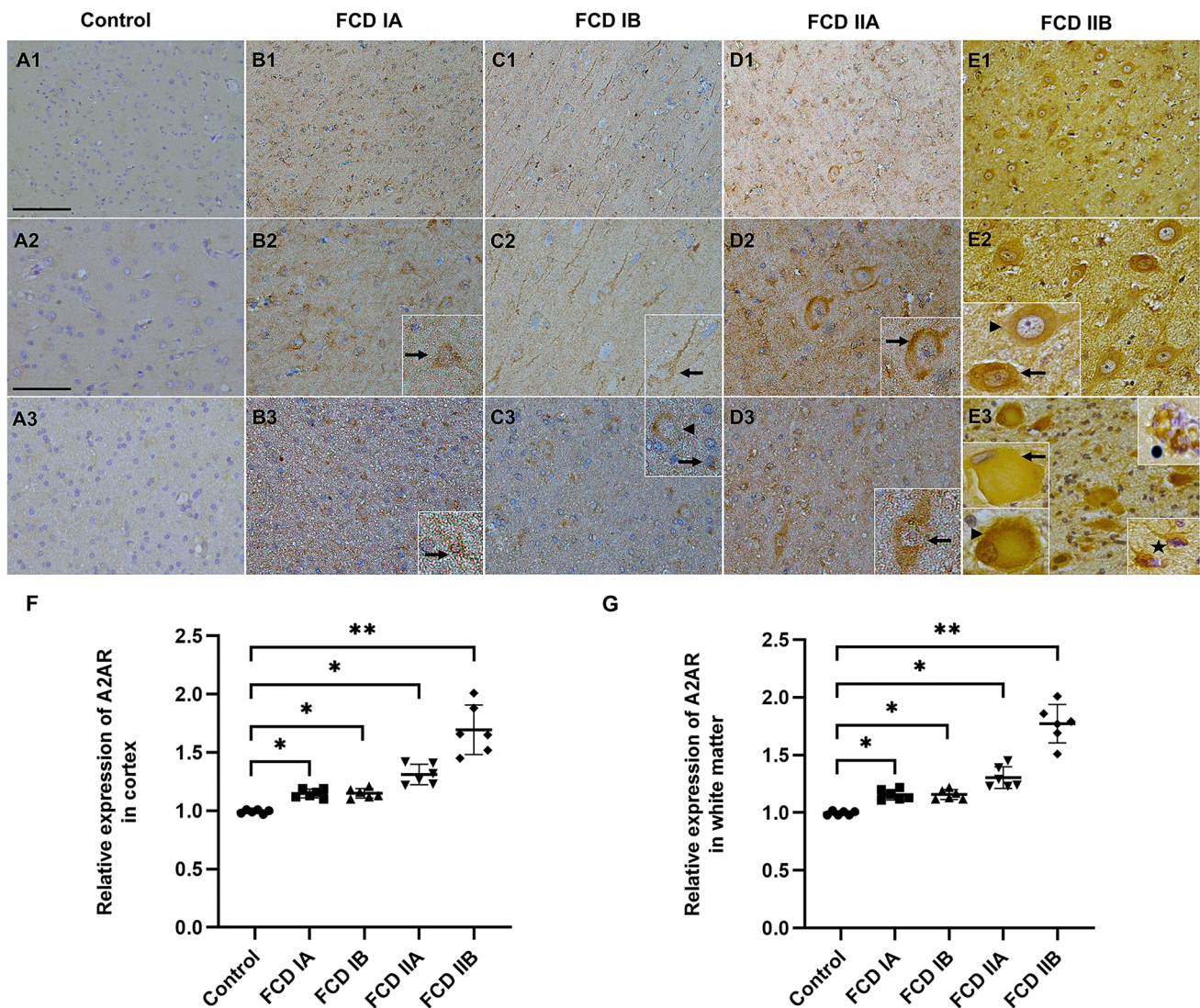
Fig. 8 Density and localization of $A_{2A}R$ within the lesions of different types of FCD. **(A1-A3)** Negative or weak density of $A_{2A}R$ in the control cortical gray matter **(A1-A2)** and the control white matter **(A3)**. **(B1-B3, C1-C3)** Within the lesions of FCD IA **(B1-B3)** and FCD IB **(C1-C3)**, we detect the perinuclear localization of $A_{2A}R$ in cells with neuronal morphology in gray matter **(B1, C1; B2, C2, arrows)**, and sparse density of $A_{2A}R$ in cells with morphology of active astrocytes **(B3, C3, arrows)**, as well as in the ectopic cells with neuronal morphology **(C3, arrowhead)** in white matter. **(D1-D3)** In the gray matter **(D1-D2)** and white matter **(D3)** within the lesions of FCD IIA, we detect perinuclear localization **(D2, arrow)** and cytoplasmic localization **(D3, arrow)** of the $A_{2A}R$ in dysmorphic enlarged neurons. **(E1-E3)** In the gray matter **(E1-E2)** and white matter **(E3)** within the lesions of FCD IIB, we find cytoplasmic localization of $A_{2A}R$ in the dysmorphic enlarged neurons **(E2, arrowhead)**, balloon cells **(E3, arrow)**, cells with microglia morphology **(E3, circle)**, and cells with morphology of reactive astrocytes **(E3, star)**. We also detect ectopic localization of $A_{2A}R$ in both the cytoplasm and the nucleus of dysmorphic enlarged neurons **(E2, arrow)** and balloon cells **(E3, arrowhead)**. Scale bars= **(A1, B1, C1, D1, E1)** 100μm; **(A2-A3, B2-B3, C2-C3, D2-D3, E2-E3)** 50μm. **(F-G)** Semiquantitative analysis of scanned immunodensities demonstrates a significant increase of $A_{2A}R$ density in both the cortex **(F)** and the white matter **(G)** of FCD compared with controls (n=6 in each group; *: $P<0.05$, **: $P<0.01$; Statistical analyses were made using unpaired two-tailed t-test; Individual data points were plotted, with error bars $\pm$ SD).

association of neuronal ADK with developmental processes in the immature brain [53]. Consistently, ADK was found to be strongly located in total cortical homogenates of the human fetal brain (gestational week 13; temporal cortex), including in deep compartments of the cortical wall (ventricular/subventricular zone) in early stages of corticogenesis [52]. Analysis of human specimens collected at autopsy and surgical controls demonstrated that ADK is weakly located in glial cells while not located in most neurons of the cortex [13, 15, 33, 50]. These results suggest that the level and density of ADK during brain development may affect important neural progenitor cell processes, including proliferation, survival, and neuroplasticity. Thus, our current findings of ectopic neuronal localization of ADK in FCD suggest an

Fig. 9 Western blot analysis of ADK and $A_{2A}R$ within the lesions of different types of FCD. (**A**) Representative immunoblots of ADK and $A_{2A}R$ in total homogenates of resected brain tissue from different types of FCD and control specimens. β-actin immunoreactivity was used to normalize for equal protein loading. (**B-C**) Quantitative analysis of ADK (**B**), and $A_{2A}R$ (**C**) levels. (n=4 in each group; **: $P<0.01$; Statistical analyses were made using unpaired two-tailed t-test; Individual data points were plotted, with error bars ± SD).
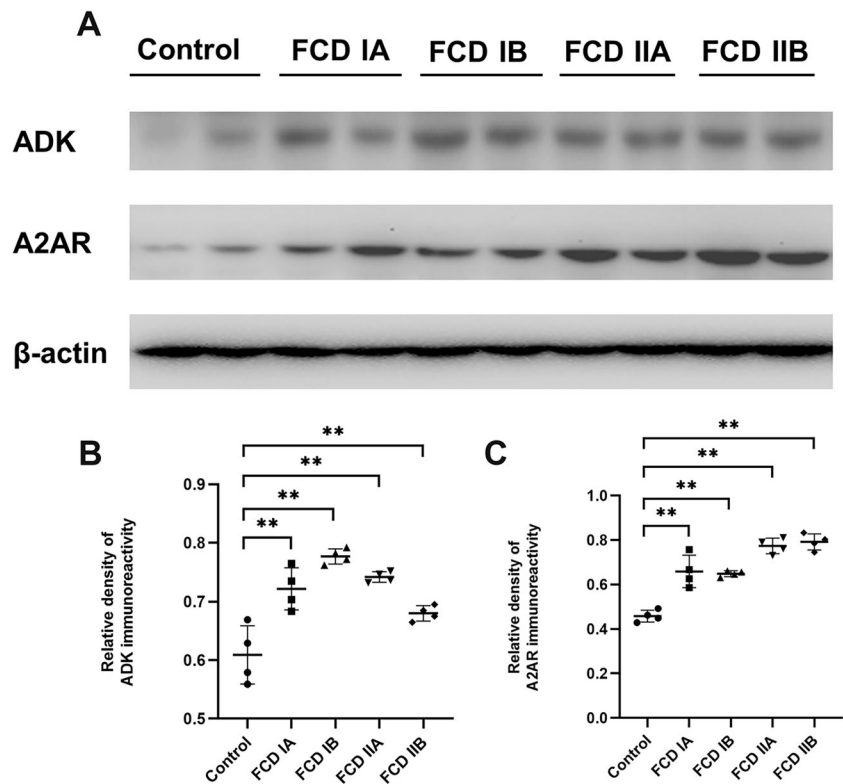
earlier, more immature localization profile of components of the adenosine system, which may indicate impaired brain maturation in FCD [52, 53]. The immature pattern of ADK localization in neurons suggests that these cells may retain a more embryonic phenotype and failed to mature fully, therefore continuing to express embryonic genes and proteins. In FCD patients, insults during the prenatal period might affect neural stem cells in the ventricular zone, leading to abnormalities in their proliferation, maturation, migration and terminal differentiation [13]. In addition to ADK, the role of $A_{2A}R$ during neurodevelopment is far better documented. According to the previous study, the density of $A_{2A}R$ is far greater (compared to any other purinergic element) in immature neurons than in adults [54]. It is not only their density but their functions are worth mentioning. $A_{2A}R$ have been shown to have a particular role during neuronal development, including the functions in the stabilization of synapses [54], in the migration of neurons [55, 56] and in defining their polarization and neurite outgrowth [56]. This is at least as important as ADK for a proper wiring of the brain and for the susceptibility to epilepsy [55]. Therefore, the increased density of $A_{2A}R$ in FCD patients might promote the epileptogenesis by affecting their neuronal development and synaptic function. We also found changes in the density of a second adenosine-metabolizing enzyme, ADA, that paralleled changes in ADK density suggesting a marked change in the extracellular adenosine pool, which is largely responsible for the activation of inhibitory A_1Rs.

While the extracellular adenosine pool is regulated by ADK and ADA, there is a distinct synaptic adenosine pool that is largely under the control of the adenosine-producing enzyme CD73 and allows the control of $A_{2A}R$ activation at the single-synapse level. In line with this association, in our present study, we found a concomitant increase in CD73 and $A_{2A}R$ immunoreactivity similar to what previously found in specimens from patients with epilepsy associated with RE, as well as patients with TLE (temporal lobe epilepsy) [27, 57]. Increased level of CD73 within FCD lesions suggests that increased CD73-mediated adenosine production might elevate the activation of $A_{2A}Rs$ in FCD. In support of increased $A_{2A}R$ activation, we also detected increased $A_{2A}R$ immunoreactivity in FCD, which might represent a compensatory response to the reduction in extracellular adenosine tone. $A_{2A}Rs$ can promote synaptic neurotoxicity by mediating the release of adenosine or its precursor ATP from neurons, thus aggravating the progression of epilepsy [58, 59]. $A_{2A}Rs$ are mainly activated through CD73-dependent adenosine production via the frequency-dependent release of ATP [23]. Different from the antiepileptic effect of A_1Rs, multiple pharmacological evidences from *in vivo* and *in vitro* studies suggest that $A_{2A}Rs$ have proconvulsive and proepileptic functions [58-62]. In the present study, we observed increased level of $A_{2A}Rs$ in reactive astrocytes, microglial cells, and neurons in FCD, which in general suggests the promotion of epileptogenesis, which may lead to further seizures [63].
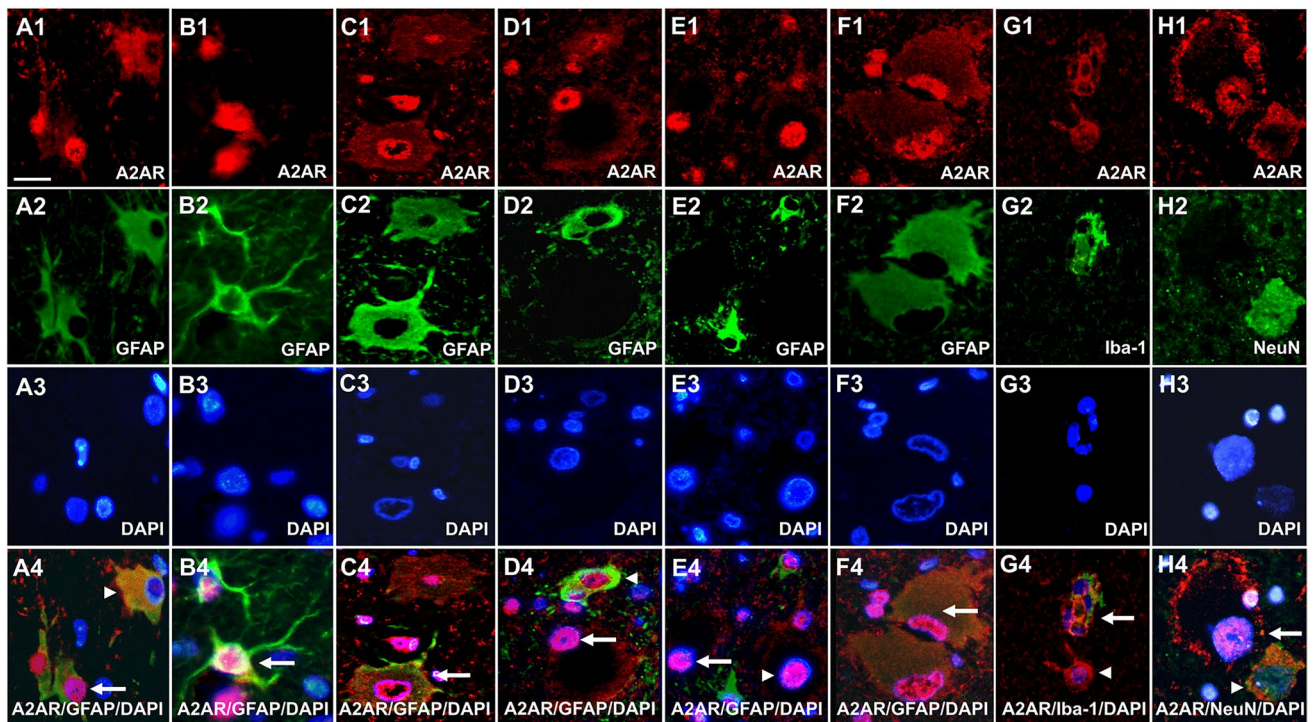
Fig. 10 Density and localization of $A_{2A}R$ in various types of cells within the lesions of FCD IIB. **(A1-A4, B1-B4)** Co-localization of $A_{2A}R$ **(A1, B1)** with GFAP **(A2, B2)** reveals nuclear localization **(A4, B4, arrows)** and cytoplasmic localization **(A4, arrowhead)** of the $A_{2A}R$ in GFAP-positive astrocytes, revealing two distinct subtypes of astrocytes: astrocytes with nuclear but no cytoplasmic $A_{2A}R$ and astrocytes with cytoplasmic, but no nuclear $A_{2A}R$. **(C1-C4)** Co-localization of $A_{2A}R$ **(C1)** with GFAP **(C2)** reveals ectopic nuclear localization of $A_{2A}R$ in GFAP-positive dysmorphic enlarged neurons **(C4, arrow)**. **(D1-D4)** Co-localization of $A_{2A}R$ **(D1)** with GFAP **(D2)** reveals nuclear localization of the $A_{2A}R$ in GFAP-negative balloon cells **(D4, arrow)** and the surrounding astrocytes **(D4, arrowhead)**. **(E1-E4)** Co-localization of $A_{2A}R$ **(E1)** with GFAP **(E2)** reveals ectopic nuclear localization of $A_{2A}R$ in GFAP-negative balloon cells **(E4, arrow)** and GFAP-negative dysmorphic enlarged neurons **(E4, arrowhead)**. **(F1-F4)** Co-localization of the $A_{2A}R$ **(F1)** with GFAP **(F2)** reveals nuclear localization of the $A_{2A}R$ in the GFAP-positive balloon cells **(F4, arrow)**. **(G1-G4)** Co-localization of $A_{2A}R$ **(G1)** with Iba-1 **(G2)** reveals cytoplasmic localization of the $A_{2A}R$ in Iba-1-positive microglia **(G4, arrow)**, as well as in Iba-1-negative cells with astrocyte morphology **(G4, arrowhead)**. **(H1-H4)** Co-localization of the $A_{2A}R$ **(H1)** with NeuN **(H2)** reveals nuclear localization of the $A_{2A}R$ in balloon cells **(H4, arrow)**, as well as a perinuclear localization in NeuN-positive neurons **(H4, arrowhead)**. **(A1, B1, C1, D1, E1, F1, G1, H1)** $A_{2A}R$ (red); **(A2, B2, C2, D2, E2, F2)** GFAP (green); **(G2)** Iba-1 (green); **(H2)** NeuN (green) **(A3, B3, C3, D3, E3, F3, G3, H3)** DAPI (blue). Scale bar=15μm.

Most researches using both selective antagonists and genetic manipulations of $A_{2A}R$ have consistently demonstrated proconvulsant effects of endogenously activated $A_{2A}R$ [61, 64-69]. There was also studies directly demonstrating that $A_{2A}R$ activation dampens A_1R function with neurochemical and electrophysiological support [21, 70]. In $A_{2A}R$ knockout mice, the severity of epileptic seizures induced by pentylenetetrazol or pilocarpine and the proportion of mice that experienced convulsions were found to be significantly reduced, indicating that activation of $A_{2A}Rs$ can modulate excitatory neurotransmission and exacerbate limbic seizures [69, 71]. Consistent with these results, the increase in $A_{2A}R$ immunoreactivity in neurons and reactive astrocytes in FCD specimens observed in the present study may indicate profound changes in $A_{2A}R$-related synaptic plasticity, neuronal excitability, and inflammation in FCD patients [72, 73].

Glutamate is the major excitatory neurotransmitter in the mammalian central nervous system, and excess extracellular glutamate plays a critical role in excitotoxicity and neuronal cell death. The astroglial glutamate transporter GLT-1, a key regulator of extracellular glutamate concentrations, mediates the uptake of glutamate by astrocytes to prevent excitotoxicity and cell death [74]. GLT-1 is under the control of $A_{2A}Rs$, which regulate astrocytic glutamate clearance through their physical associations with GLT-1 [25]. In primary cultured astrocytes as well as in an *ex vivo* preparations enriched with glial plasmalemmal vesicles, prolonged activation of $A_{2A}Rs$ led to decreased activity and density of GLT-1, thus inducing a sustained reduction in astrocytic glutamate uptake [25]. Abnormalities in astrocytic $A_{2A}R$ density and activity can therefore affect the communication between astrocytes and neurons, thereby altering glutamate homeostasis *via* regulation of GLT-1 activity[14]. This
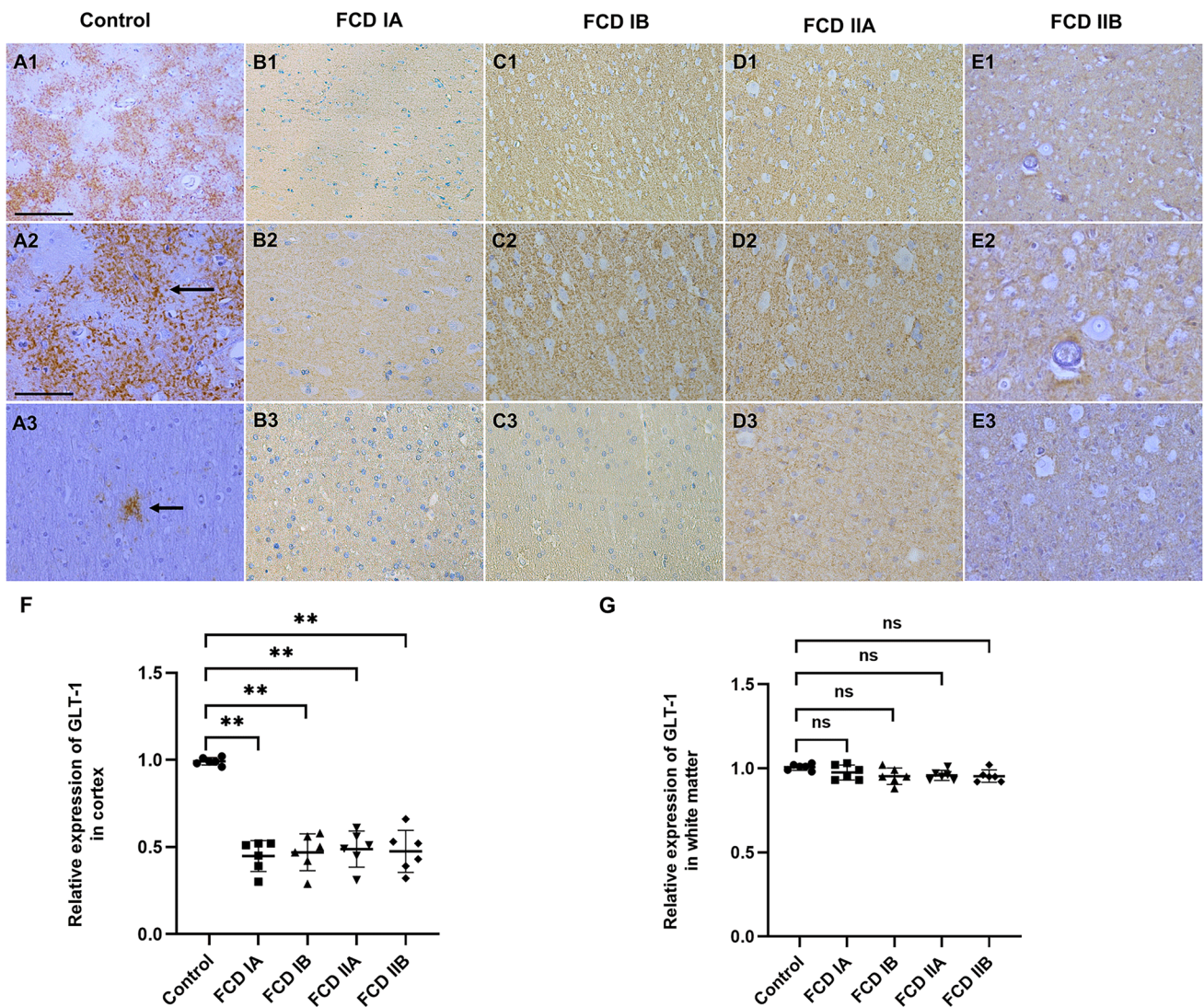
Fig. 11 Density and localization of GLT-1 within the lesions of different types of FCD. **(A1-A3)** Marked staining and patchy distribution of GLT-1 immunoreactivity detected in glial cell processes of control gray matter **(A1; A2, arrow)**. Only few GLT-1 expressing cells with astrocyte morphology in control white matter are found **(A3, arrow)**. In FCD IA **(B1-B3)**, FCD IB **(C1-C3)**, FCD IIA **(D1-D3)** and FCD IIB **(E1-E3)**, no detectable or only sparse GLT-1 density is found in cells with morphology of reactive astrocytes in the gray matter **(B1-B2, C1-C2, D1-D2, E1-E2)** and white matter **(A3, B3, C3, D3, E3)**. Scale bars= **(A1, B1, C1, D1, E1)** 100μm; **(A2-A3, B2-B3, C2-C3, D2-D3, E2-E3)** 50μm. **(F-G)** Semiquantitative analysis of scanned immunodensities demonstrates a significant decrease of GLT-1 density in the cortex **(F)** of FCD compared with controls (*n*=6 in each group; **: *P*<0.01, ns: no significance; Statistical analyses were made using unpaired two-tailed *t*-test; Individual data points were plotted, with error bars ± SD).

mechanism leads to excessive extracellular accumulation of glutamate and is thought to be involved in the pathology of neurodegenerative diseases [74]. In our previous study of specimens from RE patients, astrocytes in the brains of RE patients were found to exhibit a reduction in GLT-1 density concomitant with an increase in $A_{2A}R$ density, which might explain the increases in excitotoxicity and cell death [27]. Consistent results were also observed in the present study. An increase in $A_{2A}R$ density accompanied by a decrease in GLT-1 density in reactive astrocytes was found within lesions in the brains of FCD patients, indicating the

contribution of $A_{2A}Rs$ to the regulation of glutamate uptake in FCD. Thus, interactions between $A_{2A}Rs$ and GLT-1 may influence cell death and cognitive dysfunction associated with FCD *via* modulation of glutamate signaling, and this combined effect may be one of the key pathological bases of glutamate synaptic dysfunction and increased glutamate excitotoxicity in FCD. In addition, we found striking increased level of $A_{2A}Rs$ in reactive microglial cells in the focal lesions in FCD, suggesting a possible role of $A_{2A}Rs$ in the inflammatory response. In previous studies of FCD, the significant activation of the microglia cells was found
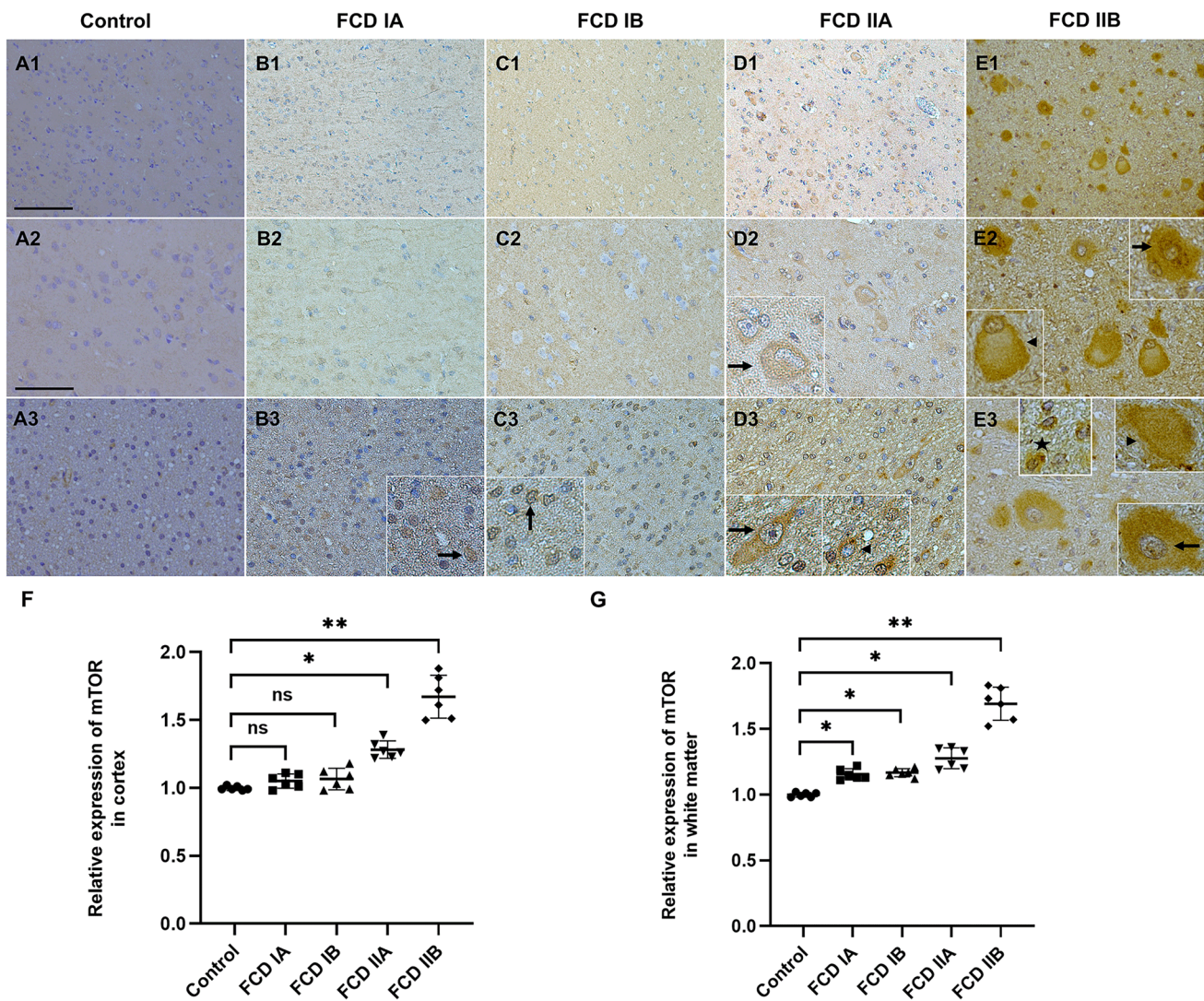
Fig. 12 Density and localization of mTOR within the lesions of different types of FCD. **(A1-A3)** Negative or weak density of mTOR in the control cortical gray matter **(A1-A2)** and the control white matter **(A3)**. **(B1-B3, C1-C3)** Within the lesions of FCD IA **(B1-B3)** and FCD IB **(C1-C3)**, mTOR is detected in cells with morphology of reactive astrocytes in the white matter **(B3, C3, arrows)**. **(D1-D3)** In the gray **(D1-D2)** and white matter **(D3)** within the lesions of FCD IIB, we detect cytoplasmic localization of mTOR in dysmorphic enlarged neurons **(D2, D3, arrows)** and cells with morphology of active astrocytes **(D3, arrowhead)**. **(E1-E3)** In the gray matter **(E1-E2)** and white matter **(E3)** within the lesions of FCD IIB, we find cytoplasmic localization of mTOR in balloon cells **(E2, E3, arrowheads)**, dysmorphic enlarged neurons **(E2, E3, arrows)**, as well as in cells with morphology of reactive astrocytes **(E3, star)**. Scale bars= **(A1, B1, C1, D1, E1)** 100µm; **(A2-A3, B2-B3, C2-C3, D2-D3, E2-E3)** 50µm. **(F-G)** Semiquantitative analysis of immunodensities demonstrates a significant increase of mTOR density in the cortex **(F)** of FCD type II, and in the white matter **(G)** of both FCD type I and II compared with controls (n=6 in each group; *: $P<0.05$, **: $P<0.01$, ns: no significance; Statistical analyses were made using unpaired two-tailed t-test; Individual data points were plotted, with error bars ± SD).

in the dysplastic cortex and strongly associated with the epileptogenicity of FCD, which was measured by seizure frequency and duration of epileptic activity[10]. Moreover, several studies in experimental models of seizures suggest a potential role of proinflammatory molecules produced by glial cells in the occurrence of seizures [75-78]. Microglia cells are an important component of glial neuropathy associated with chronic intractable epilepsy [79]. Those findings support the participation of the inflammatory response in

the epileptogenicity of FCD. The increased level of A₂ₐRs in reactive microglial cells might highlight the function of A₂ₐRs in the inflammatory response.

FCD constitutes a heterogeneous group of developmental disorders caused by germline or somatic mutations in genes modulating the PI3K/Akt/mTOR pathway [80]. mTOR is a widely located kinase that controls protein synthesis, cell size, and cell proliferation according to the availability of amino acids, growth factors, and nutrients
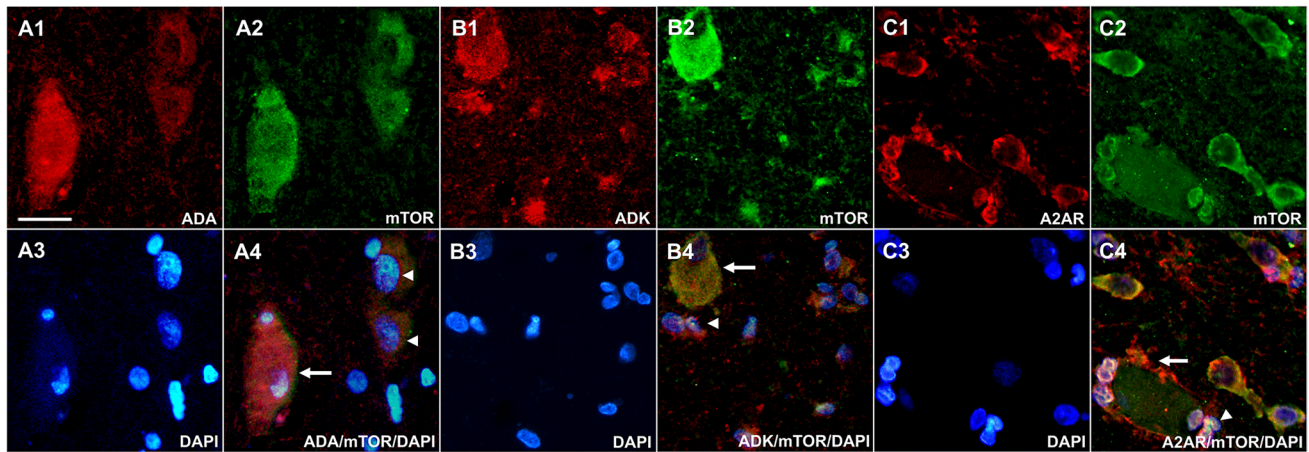
Fig. 13 Co-localization of mTOR with ADA, ADK, and $A_{2A}R$ within lesions of FCD IIB. **(A1-A4)** Co-localization of ADA **(A1)** and mTOR **(A2)** in balloon cells **(A4, arrow)** and cells with neuronal morphology **(A4, arrowheads)** within lesions of FCD IIB. **(B1-B4)** Co-localization of ADK **(B1)** and mTOR **(B2)** in balloon cells **(B4, arrow)** and cells with astrocyte morphology **(B4, arrowhead)** within lesions of FCD IIB. **(C1-C4)** Co-localization of $A_{2A}R$ **(C1)** and mTOR **(C2)** in balloon cells **(C4, arrow)** and cells with astrocyte morphology **(C4, arrowhead)** within lesions of FCD IIB. **(A1)** ADA (red); **(B1)** ADK (red); **(C1)** $A_{2A}R$ (red); **(A2, B2, C2)** mTOR (green); **(A3, B3, C3)** DAPI (blue). Scale bar=15μm.

and cell energy status [81]. Overactivation of the mTOR pathway has been found to promote epileptic seizures [82, 83]. The mTOR inhibitor rapamycin can effectively reduce the frequency and severity of epileptic seizures in patients with tuberous sclerosis [82]. AMP-activated protein kinase (AMPK), a cellular energy sensor and signal transducer regulated by a wide array of metabolic stressors, acts as an important upstream inhibitory of the mTOR pathway [84]. An increased AMP/ATP ratio *in vivo* usually indicates increased AMPK activity [85]. As an important substrate for AMP generation, adenosine may inhibit the downstream mTOR pathway through activation of AMPK, thus exerting an anticonvulsant effect [83]. In addition, the nuclear isoform of ADK may play a crucial role in the regulation of cell proliferation through a combination of epigenetic and other adenosine receptor-independent mechanisms, such as interactions with the mTOR pathway [36]. Over the past decade, increasing evidence has shown that FCD type II is associated with hyperactivation of the mTOR pathway [86]. Numerous studies have confirmed that the mTOR pathway is activated in dysmorphic enlarged neuron BCs in FCD type II patients, as well as in malformed neurons, microglia and immature cells in a variety of epilepsy-related pathologies [87, 88]. In the present study, we detected increased level of mTOR in reactive astrocytes in white matter but not the gray matter in FCD type I lesions. However, we found upregulation of mTOR in dysmorphic enlarged neurons in both the gray and white matter in FCD type IIA lesions and BCs in both the gray and white matter in FCD type IIB lesions, as well as in reactive astrocytes in both types of lesions. In addition, within FCD type IIB lesions, we found strong colocalization of mTOR

with the adenosine-metabolizing enzymes ADK and ADA and $A_{2A}Rs$. Based on the association of adenosine with the mTOR pathway, reduced adenosine concentrations in combination with attenuated inhibition of the mTOR pathway may be involved in the pathological mechanisms of epilepsy associated with FCD. In line with this notion, in a study focused on gastric cancer, the accumulation of adenosine in the hypoxic tumor microenvironment was found to activate the PI3K/Akt/mTOR signaling pathway by increasing the activation of $A_{2A}Rs$, which may enhance cancer cell stemness and promote cancer progression [37].

In conclusion, within FCD type I and type II lesions, the adenosine-metabolizing enzymes ADK and ADA and the synaptic adenosine-producing enzyme CD73 were upregulated, $A_{2A}R$ immunoreactivity was increased, and the density of putative downstream mediators of adenosine were altered, with GLT-1 density being decreased and mTOR density being increased. Together, these maladaptive changes may contribute to epileptogenesis in FCD. Our results suggest that dysregulation of the adenosine system and its downstream mediators is a common pathological feature of both FCD type I and FCD type II. Enzymes involved in adenosine metabolism as well as adenosine receptors might be potential targets for the treatment of FCD-associated epilepsy. Our descriptive findings from brain samples from FCD patients warrant the design of mechanistic studies to unravel the pathology underlying FCD-associated epilepsy.

Data Availability The datasets generated in the current research are available from the corresponding authors on reasonable request.

Declarations

Competing Interests The authors have no relevant financial or non-financial interests to disclose.

Ethics Approval This study was performed in line with the principles of the Declaration of Helsinki. Approval was granted by the local ethics committee (Beijing Sanbo Hospital, Capital Medical University, Beijing, China).

Consent for Publication Not applicable.

Consent to Participate Informed consent was obtained from parents or legal guardians of all participants.

References

1. Crino PB (2015) Focal Cortical Dysplasia. Seminars Neurol 35(3):201–8. https://doi.org/10.1055/s-0035-1552617
2. Blümcke I, Thom M, Aronica E et al (2011) The clinicopathologic spectrum of focal cortical dysplasias: a consensus classification proposed by an ad hoc Task Force of the ILAE Diagnostic Methods Commission. Epilepsia. 52(1):158–74. https://doi.org/10.1111/j.1528-1167.2010.02777.x
3. Tassi L, Garbelli R, Colombo N et al (2010) Type I focal cortical dysplasia: surgical outcome is related to histopathology. Epileptic Dis : Int Epilepsy J Videotape. 12(3):181–91. https://doi.org/10.1684/epd.2010.0327
4. Guerrini R, Duchowny M, Jayakar P et al (2015) Diagnostic methods and treatment options for focal cortical dysplasia. Epilepsia. 56(11):1669–86. https://doi.org/10.1111/epi.13200
5. Tassi L, Colombo N, Garbelli R et al (2002) Focal cortical dysplasia: neuropathological subtypes, EEG, neuroimaging and surgical outcome. Brain : J Neurol 125(Pt 8):1719–32. https://doi.org/10.1093/brain/awf175
6. Lim JS, Kim WI, Kang HC et al (2015) Brain somatic mutations in MTOR cause focal cortical dysplasia type II leading to intractable epilepsy. Nat Med 21(4):395–400. https://doi.org/10.1038/nm.3824
7. Nakashima M, Saitsu H, Takei N et al (2015) Somatic Mutations in the MTOR gene cause focal cortical dysplasia type IIb. Ann Neurol 78(3):375–86. https://doi.org/10.1002/ana.24444
8. Weichhart T, Säemann MD (2009) The multiple facets of mTOR in immunity. Trends Immunol 30(5):218–26. https://doi.org/10.1016/j.it.2009.02.002
9. Maldonado M, Baybis M, Newman D et al (2003) Expression of ICAM-1, TNF-alpha, NF kappa B, and MAP kinase in tubers of the tuberous sclerosis complex. Neurobiol Dis 14(2):279–90. https://doi.org/10.1016/s0969-9961(03)00127-x
10. Boer K, Spliet WG, van Rijen PC, Redeker S, Troost D, Aronica E (2006) Evidence of activated microglia in focal cortical dysplasia. J Neuroimmunol 173(1–2):188–95. https://doi.org/10.1016/j.jneuroim.2006.01.002
11. Cepeda C, André VM, Levine MS et al (2006) Epileptogenesis in pediatric cortical dysplasia: the dysmature cerebral developmental hypothesis. Epilepsy Behavior : E&B. 9(2):219–35. https://doi.org/10.1016/j.yebeh.2006.05.012
12. Hammers A, Koepp MJ, Richardson MP et al (2001) Central benzodiazepine receptors in malformations of cortical development: A quantitative study. Brain : J Neurol 124(Pt 8):1555–65. https://doi.org/10.1093/brain/124.8.1555
13. Luan G, Gao Q, Zhai F et al (2015) Adenosine kinase expression in cortical dysplasia with balloon cells: analysis of developmental lineage of cell types. J Neuropathol Exp Neurol 74(2):132–47. https://doi.org/10.1097/nen.0000000000000156
14. Li T, Ren G, Lusardi T et al (2008) Adenosine kinase is a target for the prediction and prevention of epileptogenesis in mice. J Clin Investig 118(2):571–82. https://doi.org/10.1172/jci33737
15. Masino SA, Li T, Theofilas P et al (2011) A ketogenic diet suppresses seizures in mice through adenosine A_1 receptors. J Clin Investig 121(7):2679–83. https://doi.org/10.1172/jci57813
16. Li T, Quan Lan J, Fredholm BB, Simon RP, Boison D (2007) Adenosine dysfunction in astrogliosis: cause for seizure generation? Neuron glia Biol 3(4):353–66. https://doi.org/10.1017/s1740925x0800015x
17. Moschovos C, Kostopoulos G, Papatheodoropoulos C (2012) Endogenous adenosine induces NMDA receptor-independent persistent epileptiform discharges in dorsal and ventral hippocampus via activation of A2 receptors. Epilepsy Res 100(1–2):157–67. https://doi.org/10.1016/j.eplepsyres.2012.02.012
18. Boison D (2016) Adenosinergic signaling in epilepsy. Neuropharmacology. 104:131–9. https://doi.org/10.1016/j.neuropharm.2015.08.046
19. Guo M, Li T (2022) Adenosine Dysfunction in Epilepsy and Associated Comorbidities. Curr Drug Targets 23(4):344–357. https://doi.org/10.2174/1389450122666210928145258
20. Guo M, Xie P, Liu S, Luan G, Li T (2022) Epilepsy and Autism Spectrum Disorder (ASD): The underlying Mechanisms and Therapy Targets related with Adenosine. Curr Neuropharmacol. https://doi.org/10.2174/1570159x20666220706100136
21. Lopes LV, Cunha RA, Kull B, Fredholm BB, Ribeiro JA (2002) Adenosine A(2A) receptor facilitation of hippocampal synaptic transmission is dependent on tonic A(1) receptor inhibition. Neuroscience. 112(2):319–29. https://doi.org/10.1016/s0306-4522(02)00080-5
22. Matos M, Augusto E, Agostinho P, Cunha RA, Chen JF (2013) Antagonistic interaction between adenosine A2A receptors and Na+/K+-ATPase-α2 controlling glutamate uptake in astrocytes. J Neurosci : Off J Soc Neurosci 33(47):18492–502. https://doi.org/10.1523/jneurosci.1828-13.2013
23. Gonçalves FQ, Lopes JP, Silva HB et al (2019) Synaptic and memory dysfunction in a β-amyloid model of early Alzheimer's disease depends on increased formation of ATP-derived extracellular adenosine. Neurobiol Dis 132:104570. https://doi.org/10.1016/j.nbd.2019.104570
24. Stockwell J, Jakova E, Cayabyab FS (2017) Adenosine A1 and A2A Receptors in the Brain: Current Research and Their Role in

Neurodegeneration. Molecules (Basel, Switzerland). 22(4)https://doi.org/10.3390/molecules22040676

25. Matos M, Augusto E, Santos-Rodrigues AD et al (2012) Adenosine A2A receptors modulate glutamate uptake in cultured astrocytes and gliosomes. Glia. 60(5):702–16. https://doi.org/10.1002/glia.22290

26. Matos M, Shen HY, Augusto E et al (2015) Deletion of adenosine A2A receptors from astrocytes disrupts glutamate homeostasis leading to psychomotor and cognitive impairment: relevance to schizophrenia. Biol Psych 78(11):763–74. https://doi.org/10.1016/j.biopsych.2015.02.026

27. He X, Chen F, Zhang Y et al (2020) Upregulation of adenosine A2A receptor and downregulation of GLT1 is associated with neuronal cell death in Rasmussen's encephalitis. Brain Pathol (Zurich, Switzerland). 30(2):246–260. https://doi.org/10.1111/bpa.12770

28. Boison D (2008) The adenosine kinase hypothesis of epileptogenesis. Progress Neurobiol 84(3):249–62. https://doi.org/10.1016/j.pneurobio.2007.12.002

29. Boison D (2012) Adenosine dysfunction in epilepsy. Glia. 60(8):1234–1243

30. Li T, Lytle N, Lan JQ, Sandau US, Boison D (2012) Local disruption of glial adenosine homeostasis in mice associates with focal electrographic seizures: a first step in epileptogenesis? Glia. 60(1):83–95. https://doi.org/10.1002/glia.21250

31. de Groot M, Iyer A, Zurolo E et al (2012) Overexpression of ADK in human astrocytic tumors and peritumoral tissue is related to tumor-associated epilepsy. Epilepsia. 53(1):58–66. https://doi.org/10.1111/j.1528-1167.2011.03306.x

32. Zhang Y, Wang X, Tang C et al (2022) Genetic variations of adenosine kinase as predictable biomarkers of efficacy of vagus nerve stimulation in patients with pharmacoresistant epilepsy. J Neurosurg. 136(3):726–735. https://doi.org/10.3171/2021.3.JNS21141

33. Luan G, Gao Q, Guan Y et al (2013) Upregulation of adenosine kinase in Rasmussen encephalitis. J Neuropathol Exp Neurol 72(11):1000–8. https://doi.org/10.1097/01.jnen.0000435369.39388.5c

34. Luan G, Wang X, Gao Q et al (2017) Upregulation of Neuronal Adenosine A1 Receptor in Human Rasmussen Encephalitis. J Neuropathol Exp Neurol 76(8):720–731. https://doi.org/10.1093/jnen/nlx053

35. Glass M, Faull RL, Bullock JY et al (1996) Loss of A1 adenosine receptors in human temporal lobe epilepsy. Brain Res. 710(1–2):56–68

36. Boison D (2013) Adenosine kinase: exploitation for therapeutic gain. Pharmacol Rev 65(3):906–43. https://doi.org/10.1124/pr.112.006361

37. Shi L, Wu Z, Miao J et al (2019) Adenosine interaction with adenosine receptor A2a promotes gastric cancer metastasis by enhancing PI3K-AKT-mTOR signaling. Mole Biol Cell 30(19):2527–2534. https://doi.org/10.1091/mbc.E19-03-0136

38. Liu G, Yang S, Liu Y et al (2022) The adenosine-A2a receptor regulates the radioresistance of gastric cancer via PI3K-AKT-mTOR pathway. Int J Clin Oncol 27(5):911–920. https://doi.org/10.1007/s10147-022-02123-x

39. Palmini A, Najm I, Avanzini G et al (2004) Terminology and classification of the cortical dysplasias. Neurology. 62(6 Suppl 3):S2-8. https://doi.org/10.1212/01.wnl.0000114507.30388.7e

40. Luan G, Gao Q, Zhai F, Chen Y, Li T (2016) Upregulation of HMGB1, toll-like receptor and RAGE in human Rasmussen's encephalitis. Epilepsy Res 123:36–49. https://doi.org/10.1016/j.eplepsyres.2016.03.005

41. Bautista JF, Lüders HO (2000) Semiological seizure classification: relevance to pediatric epilepsy. Epileptic Disord : Int epilepsy J Videotape. 2(1):65-72; discussion 73

42. Lüders H, Acharya J, Baumgartner C et al (1998) Semiological seizure classification. Epilepsia. 39(9):1006–13. https://doi.org/10.1111/j.1528-1157.1998.tb01452.x

43. Li T, Steinbeck JA, Lusardi T et al (2007) Suppression of kindling epileptogenesis by adenosine releasing stem cell-derived brain implants. Brain : J Neurol 130(Pt 5):1276–88. https://doi.org/10.1093/brain/awm057

44. Yegutkin GG, Boison D (2022) ATP and Adenosine Metabolism in Cancer: Exploitation for Therapeutic Gain. Pharmacol Rev 74(3):797–822. https://doi.org/10.1124/pharmrev.121.000528

45. Boison D, Yegutkin GG (2019) Adenosine metabolism: emerging concepts for cancer therapy. Cancer Cell 36:582–596

46. During MJ, Spencer DD (1992) Adenosine: a potential mediator of seizure arrest and postictal refractoriness. Ann Neurol 32(5):618–24

47. Boison D, Chen JF, Fredholm BB (2010) Adenosine signaling and function in glial cells. Cell Death Differ. 17(7):1071–82. https://doi.org/10.1038/cdd.2009.131

48. Fedele DE, Koch P, Brüstle O et al (2004) Engineering embryonic stem cell derived glia for adenosine delivery. Neurosci Lett. 370(2–3):160–165

49. Patodia S, Paradiso B, Garcia M et al (2020) Adenosine kinase and adenosine receptors A(1) R and A(2A) R in temporal lobe epilepsy and hippocampal sclerosis and association with risk factors for SUDEP. Epilepsia. 61(4):787–797. https://doi.org/10.1111/epi.16487

50. Aronica E, Zurolo E, Iyer A et al (2011) Upregulation of adenosine kinase in astrocytes in experimental and human temporal lobe epilepsy. Epilepsia. 52(9):1645–55. https://doi.org/10.1111/j.1528-1167.2011.03115.x

51. Cui XA, Singh B, Park J, Gupta RS (2009) Subcellular localization of adenosine kinase in mammalian cells: The long isoform of AdK is localized in the nucleus. Biochem Biophys Res Commun 388(1):46–50. https://doi.org/10.1016/j.bbrc.2009.07.106

52. Aronica E, Sandau US, Iyer A, Boison D (2013) Glial adenosine kinase–a neuropathological marker of the epileptic brain. Neurochem Int 63(7):688–95. https://doi.org/10.1016/j.neuint.2013.01.028

53. Studer FE, Fedele DE, Marowsky A, et al (2006) Shift of adenosine kinase expression from neurons to astrocytes during postnatal development suggests dual functionality of the enzyme. *Neuroscience*. 142(1):125-37. S0306-4522(06)00812-8 [pii] https://doi.org/10.1016/j.neuroscience.2006.06.016

54. Gomez-Castro F, Zappettini S, Pressey JC et al (2021) Convergence of adenosine and GABA signaling for synapse stabilization during development. Science (New York, NY) 374(6568):eabk2055. https://doi.org/10.1126/science.abk2055

55. Silva CG, Métin C, Fazeli W et al (2013) Adenosine receptor antagonists including caffeine alter fetal brain development in mice. Sci Transl Med 5(197):197ra104. https://doi.org/10.1126/scitranslmed.3006258

56. Alçada-Morais S, Gonçalves N, Moreno-Juan V et al (1991) 2021 Adenosine A2A Receptors Contribute to the Radial Migration of Cortical Projection Neurons through the Regulation of Neuronal Polarization and Axon Formation. Cerebral Cortex (New York, NY 1991) 31(12):5652–5663. https://doi.org/10.1093/cercor/bhab188

57. Barros-Barbosa AR, Ferreirinha F, Oliveira Â et al (2016) Adenosine A(2A) receptor and ecto-5'-nucleotidase/CD73 are upregulated in hippocampal astrocytes of human patients with mesial temporal lobe epilepsy (MTLE). Purinergic Signal 12(4):719–734. https://doi.org/10.1007/s11302-016-9535-2

58. Silva CG, Porciúncula LO, Canas PM, Oliveira CR, Cunha RA (2007) Blockade of adenosine A(2A) receptors prevents staurosporine-induced apoptosis of rat hippocampal neurons. Neurobiol Dis 27(2):182–9. https://doi.org/10.1016/j.nbd.2007.04.018

59. Popoli P, Frank C, Tebano MT et al (2003) Modulation of glutamate release and excitotoxicity by adenosine A2A receptors. Neurology. 61(11 Suppl 6):S69-71. https://doi.org/10.1212/01.wnl.0000095216.89483.a2

60. D'Alimonte I, D'Auro M, Citraro R et al (2009) Altered distribution and function of A2A adenosine receptors in the brain of WAG/Rij rats with genetic absence epilepsy, before and after appearance of the disease. Eur J Neurosci 30(6):1023–35. https://doi.org/10.1111/j.1460-9568.2009.06897.x

61. Li X, Kang H, Liu X, et al 2012 Effect of adenosine A2A receptor antagonist ZM241385 on amygdala-kindled seizures and progression of amygdala kindling. Journal of Huazhong University of Science and Technology Medical sciences = Hua zhong ke ji da xue xue bao Yi xue Ying De wen ban = Huazhong keji daxue xuebao Yixue Yingdewen ban. 32(2):257-264. https://doi.org/10.1007/s11596-012-0046-2

62. Tescarollo FC, Rombo DM, DeLiberto LK et al (2020) Role of Adenosine in Epilepsy and Seizures. J Caffeine Adenosine Res 10(2):45–60. https://doi.org/10.1089/caff.2019.0022

63. Xu X, Beleza RO, Gonçalves FQ et al (2022) Adenosine A(2A) receptors control synaptic remodeling in the adult brain. Sci Rep 12(1):14690. https://doi.org/10.1038/s41598-022-18884-4

64. El Yacoubi M, Ledent C, Parmentier M, Daoust M, Costentin J, Vaugeois J (2001) Absence of the adenosine A(2A) receptor or its chronic blockade decrease ethanol withdrawal-induced seizures in mice. Neuropharmacology. 40(3):424–32. https://doi.org/10.1016/s0028-3908(00)00173-8

65. El Yacoubi M, Ledent C, Parmentier M, Costentin J, Vaugeois JM (2008) Evidence for the involvement of the adenosine A(2A) receptor in the lowered susceptibility to pentylenetetrazol-induced seizures produced in mice by long-term treatment with caffeine. Neuropharmacology. 55(1):35–40. https://doi.org/10.1016/j.neuropharm.2008.04.007

66. Hosseinmardi N, Mirnajafi-Zadeh J, Fathollahi Y, Shahabi P (2007) The role of adenosine A1 and A2A receptors of entorhinal cortex on piriform cortex kindled seizures in rats. Pharmacol Res 56(2):110–7. https://doi.org/10.1016/j.phrs.2007.04.011

67. Zeraati M, Mirnajafi-Zadeh J, Fathollahi Y, Namvar S, Rezvani ME (2006) Adenosine A1 and A2A receptors of hippocampal CA1 region have opposite effects on piriform cortex kindled seizures in rats. Seizure. 15(1):41–8. https://doi.org/10.1016/j.seizure.2005.10.006

68. Etherington LA, Frenguelli BG (2004) Endogenous adenosine modulates epileptiform activity in rat hippocampus in a receptor subtype-dependent manner. Eur J Neurosci 19(9):2539–50. https://doi.org/10.1111/j.0953-816X.2004.03355.x

69. El Yacoubi M, Ledent C, Parmentier M, Costentin J, Vaugeois JM (2009) Adenosine A2A receptor deficient mice are partially resistant to limbic seizures. Naunyn-Schmiedeberg's arch Pharmacol 380(3):223–32. https://doi.org/10.1007/s00210-009-0426-8

70. Lopes LV, Cunha RA, Ribeiro JA (1999) Cross talk between A(1) and A(2A) adenosine receptors in the hippocampus and cortex of young adult and old rats. J Neurophysiol 82(6):3196–203. https://doi.org/10.1152/jn.1999.82.6.3196

71. Canas PM, Porciúncula LO, Simões AP, et al (2018) Neuronal Adenosine A2A Receptors Are Critical Mediators of Neurodegeneration Triggered by Convulsions. eNeuro. 5(6) https://doi.org/10.1523/eneuro.0385-18.2018

72. Cunha RA (2016) How does adenosine control neuronal dysfunction and neurodegeneration? J Neurochem 139(6):1019–1055. https://doi.org/10.1111/jnc.13724

73. Gomes CV, Kaster MP, Tome AR, Agostinho PM, Cunha RA (2011) Adenosine receptors and brain diseases: neuroprotection and neurodegeneration. Biochim Biophys Acta. May 1808(5):1380-99. S0005-2736(10)00423-2 [pii] https://doi.org/10.1016/j.bbamem.2010.12.001

74. Benarroch EE (2010) Glutamate transporters: diversity, function, and involvement in neurologic disease. Neurology. 74(3):259–64. https://doi.org/10.1212/WNL.0b013e3181cc89e3

75. Aronica E, van Vliet EA, Hendriksen E, Troost D, Lopes da Silva FH, Gorter JA (2001) Cystatin C, a cysteine protease inhibitor, is persistently up-regulated in neurons and glia in a rat model for mesial temporal lobe epilepsy. The European journal of neuroscience 14(9):1485–91. https://doi.org/10.1046/j.0953-816x.2001.01779.x

76. Beach TG, Woodhurst WB, MacDonald DB, Jones MW (1995) Reactive microglia in hippocampal sclerosis associated with human temporal lobe epilepsy. Neurosci Lett 191(1–2):27–30. https://doi.org/10.1016/0304-3940(94)11548-1

77. Niquet J, Ben-Ari Y, Represa A (1994) Glial reaction after seizure induced hippocampal lesion: immunohistochemical characterization of proliferating glial cells. J Neurocytol 23(10):641–56. https://doi.org/10.1007/bf01191558

78. Taniwaki Y, Kato M, Araki T, Kobayashi T (1996) Microglial activation by epileptic activities through the propagation pathway of kainic acid-induced hippocampal seizures in the rat. Neurosci Lett 217(1):29–32. https://doi.org/10.1016/0304-3940(96)13062-7

79. Aronica E, Gorter JA, Redeker S et al (2005) Distribution, characterization and clinical significance of microglia in glioneuronal tumours from patients with chronic intractable epilepsy. Neuropathol Appl Neurobiol 31(3):280–91. https://doi.org/10.1111/j.1365-2990.2004.00636.x

80. Iffland PH 2nd, Crino PB (2017) Focal Cortical Dysplasia: Gene Mutations, Cell Signaling, and Therapeutic Implications. Ann Rev Pathol 12:547–571. https://doi.org/10.1146/annurev-pathol-052016-100138

81. Mossmann D, Park S, Hall MN (2018) mTOR signalling and cellular metabolism are mutual determinants in cancer. Nat Rev Cancer. 18(12):744–757. https://doi.org/10.1038/s41568-018-0074-8

82. Curatolo P, Moavero R, van Scheppingen J, Aronica E (2018) mTOR dysregulation and tuberous sclerosis-related epilepsy. Exp Rev Neurotherapeut 18(3):185–201. https://doi.org/10.1080/14737175.2018.1428562

83. Hodges SL, Lugo JN (2020) Therapeutic role of targeting mTOR signaling and neuroinflammation in epilepsy. Epilepsy Res 161:106282. https://doi.org/10.1016/j.eplepsyres.2020.106282

84. Inoki K, Kim J, Guan KL (2012) AMPK and mTOR in cellular energy homeostasis and drug targets. Ann Rev Pharmacol Toxicol 52:381–400. https://doi.org/10.1146/annurev-pharmtox-010611-134537

85. Yan Y, Mukherjee S, Harikumar KG et al (2021) Structure of an AMPK complex in an inactive, ATP-bound state. Science (New York, NY). 373(6553):413–419. https://doi.org/10.1126/science.abe7565

86. Marsan E, Baulac S (2018) Review: Mechanistic target of rapamycin (mTOR) pathway, focal cortical dysplasia and epilepsy. Neuropathol Appl Neurobiol 44(1):6–17. https://doi.org/10.1111/nan.12463

87. Ljungberg MC, Bhattacharjee MB, Lu Y et al (2006) Activation of mammalian target of rapamycin in cytomegalic neurons of human cortical dysplasia. Ann Neurol 60(4):420–9. https://doi.org/10.1002/ana.20949

88. Liu J, Reeves C, Michalak Z et al (2014) Evidence for mTOR pathway activation in a spectrum of epilepsy-associated pathologies. Acta Neuropathol Commun 2:71. https://doi.org/10.1186/2051-5960-2-71